THE ASTROPHYSICAL JOURNAL, 544:218–241, 2000 November 20

MULTIWAVELENGTH OBSERVATIONS OF DUSTY STAR FORMATION AT LOW AND HIGH REDSHIFT

KURT L. ADELBERGER AND CHARLES C. STEIDEL[1,2]
Palomar Observatory, Caltech 105-24, Pasadena, CA 91125
Received 2000 January 7; accepted 2000 June 23

ABSTRACT

If high-redshift galaxies resemble rapidly star-forming galaxies in the local universe, most of the luminosity produced by their massive stars will have been absorbed by dust and reradiated as far-infrared photons that cannot be detected with existing facilities. This paper examines what can be learned about high-redshift star formation from the small fraction of high-redshift galaxies' luminosities that is emitted at accessible wavelengths. We first consider the most basic ingredient in the analysis of high-redshift surveys: the estimation of star formation rates for detected galaxies. Standard techniques require an estimate of the bolometric luminosity produced by their massive stars. We review and quantify empirical correlations between bolometric luminosities produced by star formation and the UV, mid-IR, sub-mm, and radio luminosities of galaxies in the local universe. These correlations suggest that observations of high-redshift galaxies at any of these wavelengths should constrain their star formation rates to within $\sim$0.2–0.3 dex. We assemble the limited evidence that high-redshift galaxies obey these locally calibrated correlations. The second part of the paper assesses whether existing surveys have found the galaxies that host the majority of star formation at high redshift even though they directly detect only a small fraction of the luminosities of individual galaxies. We describe the characteristic luminosities and dust obscurations of galaxies at $z \sim 0$, $z \sim 1$, and $z \sim 3$. After discussing the relationship between the high-redshift populations selected in surveys at different wavelengths, we calculate the contribution to the 850 μm background from each and argue that these known galaxy populations can together have produced the entire observed background. The available data show that a correlation between star formation rate and dust obscuration $L_{\rm bol,\,dust}/L_{\rm UV}$ exists at low and high redshift alike. The existence of this correlation plays a central role in the major conclusion of this paper: most star formation at high redshift occurred in galaxies with moderate dust obscurations $1 \lesssim L_{\rm bol,\,dust}/L_{\rm UV} \lesssim 100$ similar to those that host the majority of star formation in the local universe and to those that are detected in UV-selected surveys.

Subject headings: dust, extinction — galaxies: evolution — galaxies: formation — galaxies: ISM — galaxies: starburst

On-line material: color figures

1. INTRODUCTION

The universe of galaxies beyond $z \sim 1$ has finally become relatively easy to observe. While only a handful of galaxies at $z \gtrsim 1$ were known 5 years ago, close to 2000 have spectroscopic redshifts today. Planned redshift surveys should increase the number by at least an order of magnitude in the next several years. Analyzing the large and rapidly growing samples of high-redshift galaxies will be a major challenge in the coming decade.

Much of this analysis will rely on estimates of star formation rates for the detected galaxies. These estimates are required to answer the most basic questions that high-redshift surveys can address—when did the stars in the universe form? how were the sites of star formation related to the evolving perturbations in the underlying distribution of matter?—but unfortunately no standard and widely accepted techniques exist for estimating star formation rates from the data usually available in high-redshift samples. Researchers analyzing data taken at a variety of wavelengths with a variety of techniques have reached wildly discrepant conclusions about the star formation history of the universe (e.g., Madau et al. 1996; Smail, Ivison, & Blain 1997; Barger et al. 1998; Blain et al. 1999a, 1999c; Eales et al. 1999; Pettini et al. 1999; Steidel et al. 1999; Tan, Silk, & Balland 1999; Trentham, Blain, & Goldader 1999; Barger, Cowie, & Richards 2000, hereafter BCR).

The central problem is that the energy produced by star formation in young galaxies is emitted across more than 6 decades of frequency, from the far-UV to the radio, while most high-redshift surveys are based on observations at only a narrow range of frequencies. Standard methods for deriving a galaxy's star formation rate require an estimate of the total energy emitted by its massive stars, but in existing surveys this is never directly observed. Radio surveys detect only the tiny percentage of the total energy that goes into accelerating electrons in supernova remnants, for example, while optical surveys detect the portion of massive stars' emission that is not absorbed by dust and sub-mm surveys detect a fraction of the portion that is. Large and uncertain corrections are needed to estimate the total emitted energy from the energy detected at any of these wavelengths. Differences in the adopted corrections are largely responsible for current discrepancies in estimates of the star formation history of the universe.

In principle one could obtain a robust estimate of the energy emitted by massive stars in a high-redshift galaxy by observing it over a sufficiently wide range of wavelengths, but with current technology this is rarely possible. Star-forming galaxies at high redshift almost certainly emit the bulk of their luminosities at far-infrared wavelengths that are extremely difficult to detect. Although massive stars

[1] NSF Young Investigator.
[2] Packard Fellow.

themselves radiate mainly in the far-UV, rapid star formation in the local universe occurs in dusty environments where most UV photons are quickly absorbed, and as a result most of the luminosity produced by massive stars tends to emerge in the far-IR where dust radiates. This is known to be true for a broad range of galaxies in the local universe, from the famous class of "ultra luminous infrared galaxies" (ULIRGs, galaxies with $L_{\rm FIR} \gtrsim 10^{12}\ L_\odot$) to the much fainter UV-selected starbursts contained in the *IUE* Atlas (e.g., Meurer, Heckman, & Calzetti 1999, hereafter MHC). The recent detection of a large extragalactic far-IR background (e.g., Fixsen et al. 1998) suggests that it is likely to have been true at high redshifts as well.

Because most of the energy produced by massive stars is likely radiated by dust in the far-IR, estimates of the bolometric dust luminosities of high-redshift galaxies are required in order to estimate their star formation rates. The bolometric dust luminosities usually cannot be directly observed—Earth's atmosphere is opaque in the far-IR and most high-redshift galaxies are too faint to have been detected by any far-IR satellite that has flown—but they can be inferred from known correlations between local galaxies' bolometric dust luminosities and their luminosities in the optical, mid-IR, sub-mm, and radio atmospheric windows.

The first part of this paper aims to present a unified framework for estimating the bolometric dust luminosities of high-redshift galaxies selected at different wavelengths. In § 2 we summarize and reexamine locally established correlations between bolometric dust luminosities and luminosities through atmospheric windows, quantifying their scatter in cases where it has not been done explicitly by previous authors. In § 3 we present the limited available evidence that high-redshift galaxies obey these correlations. Published estimates of the cosmic star formation history derived from observations through one atmospheric window have often been accompanied by claims that most of the star formation could not have been detected with observations through other atmospheric windows. In the second part of this paper, § 4, we use the results of §§ 2 and 3 to evaluate whether this is true. After reviewing the properties of star-forming galaxies in the local universe, we discuss the properties of high-redshift galaxies selected in surveys at different wavelengths and estimate the contribution to the far-IR background from galaxies similar to those detected in optical, mid-IR, and sub-mm surveys. Our conclusions are presented in § 5.

Throughout this paper we shall denote luminosities by L when they have units of energy time^{-1}, by l_ν when they have units of energy time^{-1} frequency^{-1}, and by l_λ when they have units of energy time^{-1} wavelength^{-1}; and observed fluxes by f_ν (units of energy time^{-1} frequency^{-1} area^{-1}) or f_λ (units of energy time^{-1} wavelength^{-1} area^{-1}).

2. DUST-OBSCURED STAR FORMATION IN THE LOCAL UNIVERSE

The energy produced by massive stars emerges from galaxies over a wide range of wavelengths. Figure 1 shows typical spectral shapes of this emission for rapidly star-forming galaxies in the local universe. Massive stars radiate predominantly in the far-UV, but as galaxies become dustier an ever larger fraction of their luminosity is absorbed by dust and reradiated in the far-IR. In typical cases most of the energy released by massive stars emerges

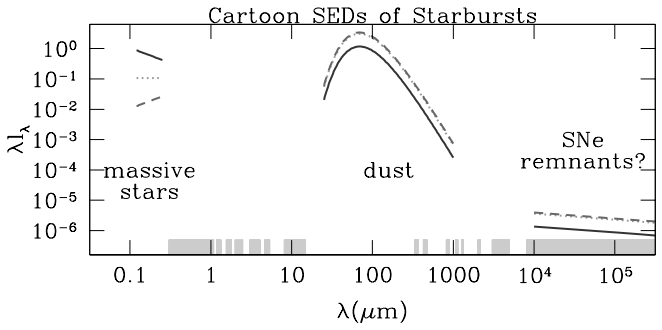

FIG. 1.—Schematic spectra of a starburst with fixed star formation rate and varying dust opacity. These spectra illustrate the empirical correlations between UV, far-IR, and radio properties of actively star-forming galaxies in the local universe. Increasing the dust obscuration makes the UV continuum redder and fainter while boosting the far-IR luminosity; increases in far-IR luminosity are accompanied by increases in radio luminosity. The range of obscurations shown ($A_{1600} \sim 0.5$, *solid line*; $A_{1600} \sim 2.5$, *dotted line*; $A_{1600} \sim 4.5$, *dashed line*) roughly span the range observed in local starbursts. At $A_{1600} \sim 2.5$ most of the luminosity of massive stars is absorbed by dust. Further increases in dust opacity do not significantly increase the absorbed energy, and so the dotted and dashed lines nearly overlap in the far-IR and radio. Dust emission in the far-IR is typically the dominant component in rapidly star-forming galaxies bolometric luminosities, but most of this emission cannot be detected through atmospheric windows (*shaded regions on the lower abscissa*). See the electronic edition of the Journal for a color version of this figure.

in the far-IR. This section describes how the dust's bolometric luminosity can be estimated from observations through the atmospheric windows indicated on the x-axis of Figure 1.

2.1. *Sub-mm Constraints on Bolometric Dust Luminosity*

Although a galaxy's total dust luminosity at 10 μm $\lesssim \lambda \lesssim$ 1000 μm cannot be directly measured from the ground, narrow atmospheric windows in the sub-millimeter (Fig. 1) allow a small fraction of it to reach the Earth's surface. If dust in all galaxies radiated with the same known spectral energy distribution (SED)—say a 50 K blackbody—then a galaxy's bolometric dust luminosity could be reliably estimated by simply scaling the flux measured through a sub-mm atmospheric window.[3] Unfortunately, dust SEDs vary considerably from one galaxy to the next and are more complex than simple blackbodies. Obtaining a reasonable fit to a galaxy's measured dust SED usually requires at least two "modified" blackbodies of the form

$$f_\nu \propto \frac{\nu^{3+\epsilon}}{\exp\,(h\nu/kT) - 1}\,, \tag{1}$$

where $\epsilon \sim 1.5$, the emissivity index, is sometimes treated as a free parameter in addition to the temperatures and amplitudes of the modified blackbodies (e.g., Klaas et al. 1997). The required parameters in these fits vary among galaxies in a way that is not quantitatively understood.

Because of the significant variation in the shape of galaxies' dust SEDs, measuring a galaxy's flux in one of the narrow sub-mm atmospheric windows cannot precisely determine its bolometric dust luminosity. Nevertheless, sub-mm fluxes provide some useful information; galaxies with large fluxes through the sub-mm atmospheric windows tend also to have large bolometric dust luminosities. To

[3] Provided, of course, that the galaxy's redshift and luminosity distance are known.

quantify how well sub-mm flux measurements can constrain the bolometric dust luminosities of actively star-forming galaxies in the local universe, we have assembled from the literature a sample of these galaxies with published *IRAS* fluxes at 25, 60, and 100 μm, as well as at least one flux measurement at a wavelength 200 $\mu\text{m} < \lambda < 1000$ μm to constrain the temperature of the cool dust component and the slope of its (modified) Rayleigh-Jeans tail. This sample consists of 27 galaxies: the ULIRGs IRAS 05189-2524, IRAS 08572+3915, UGC 5101, IRAS 12112+0305, Mrk 231, Mrk 273, IRAS 14348-1447, and IRAS 15250+3609 detected at 800 μm (and sometimes 450 μm) by Rigopoulou et al. (1996); the LIRGs NGC 1614, NGC 3110, NGC 4194, NGC 4418, NGC 5135, NGC 5256, NGC 5653, NGC 5936, Arp 193, and Zw 049 detected at 850 μm by Lisenfeld, Isaak, & Hills 2000; the interacting galaxies NGC 6240, Arp 220, and Arp 244 observed at 25 $\mu\text{m} < \lambda < 200$ μm by Klaas et al. (1997); the UV-selected starbursts NGC 6090, NGC 7673, NGC 5860, IC 1586, and Tol 1924-416 detected at 150 and 205 μm by Calzetti et al. (1999); and the nearby starburst M82 (Hughes, Gear, & Robson 1990 and references therein).

The dust SEDs of these galaxies are shown in Figure 2. For clarity we have connected measurements of individual galaxies at different wavelengths with spline fits (*continuous lines*). These fits were calculated in $\log \lambda - \log f_\lambda$ space and should roughly capture the expected power-law shape of dust SEDs in their (modified) Rayleigh-Jeans tails. Measurements from all galaxies were normalized to have the same total luminosity under the fits.

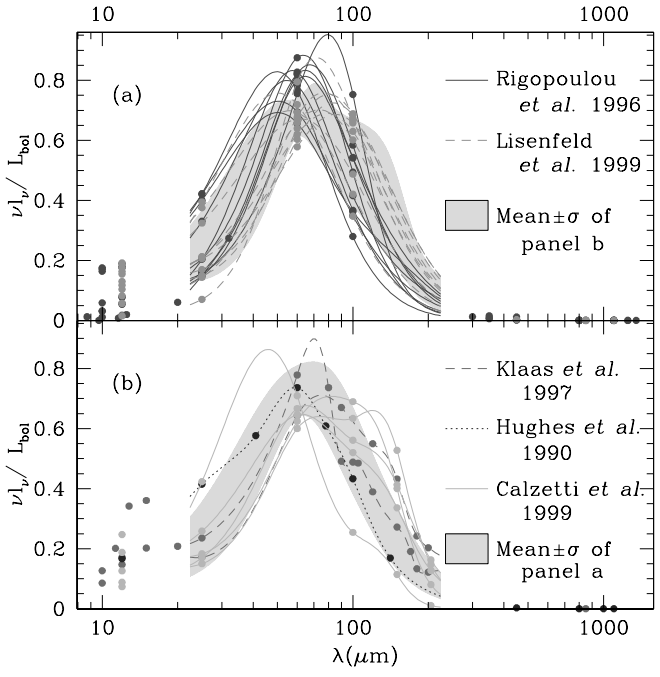

FIG. 2.—Far-IR spectral energy distributions of plausible local analogs to rapidly star-forming high-redshift galaxies. The points show measurements (see text for references) and the solid lines spline fits to these measurements. Each SED has been scaled to have the same total luminosity within the range of the spline fit. Panel (*a*) shows the dust SEDs of galaxies with unusually large IR luminosities (LIRGs and ULIRGs). Panel (*b*) shows galaxies where more detailed dust SED measurements are available; these are mainly less luminous UV-selected galaxies. The dust SEDs of these two samples are not drastically different, as the shaded regions show. Because of the range in $\nu l_\nu / L_{bol}$ at each wavelength, measuring a galaxy's flux at only one far-IR/sub-mm wavelength cannot pin down precisely its bolometric dust luminosity. This statement is quantified in § 2.1 and Table 1. See the electronic edition of the Journal for a color version of this figure.

This plot can be used to estimate a rapidly star-forming galaxy's bolometric dust luminosity on the basis of its luminosity at a single observed wavelength:

$$L_{\text{bol, dust}} \sim \left\langle \frac{L_{\text{bol, dust}}}{\lambda l_\lambda} \right\rangle \lambda l_\lambda \equiv \mathcal{K}(\lambda) \lambda l_\lambda \, , \qquad (2)$$

where the expectation value is taken over all dust SEDs in the figure. Table 1 lists the values $\mathcal{K}$ at various wavelengths. Ideally, one would calculate $\mathcal{K}$ by fitting two modified blackbodies to each dust SED, as discussed above, but most of the galaxies in our sample have measured fluxes at only four relevant wavelengths (25, 60, 100, and 850 μm) and this fit has more than four free parameters. Instead, we estimated $\mathcal{K}$ from the log-log spline interpolations shown in Figure 2. This spline fitting does not take proper account of uncertainties in the measured fluxes, but the uncertainties are almost always far smaller than the intrinsic differences in dust SEDs among the galaxies in our sample. The observed spread among these galaxies in $L_{\text{bol, dust}}/\lambda l_\lambda$ at a given wavelength provides a measure of how reliably a flux measurement at that wavelength can constrain a galaxy's bolometric dust luminosity. The rms spread in $\log_{10} \mathcal{K}$, also listed in Table 1, suggests sub-mm estimates of $L_{\text{bol, dust}}$ will be accurate to about a factor of 2.

According to Sanders & Mirabel (1996) and Dunne et al. (2000), the shapes of galaxies' dust SEDs are correlated with their bolometric luminosities, and so one might hope to estimate $L_{\text{bol, dust}}$ more accurately by using different values of $\mathcal{K}$ for galaxies with different absolute sub-mm luminosities. Unfortunately, this trend does not appear to be

TABLE 1

LOCAL DUST SEDs[a]

λ (μm)	$\langle 1/\mathcal{K}_\lambda \rangle$	$\sigma_{\mathcal{K}}$(dex)	N_{objects}
25.....	0.25	0.21	27
50.....	0.64	0.08	27
75.....	0.69	0.06	27
100.....	0.53	0.12	27
125.....	0.38	0.17	27
150.....	0.26	0.22	27
175.....	0.17	0.25	27
200.....	0.11	0.30	27
225.....	0.076	0.30	21
250.....	0.055	0.31	21
275.....	0.041	0.32	21
300.....	0.030	0.32	21
325.....	0.023	0.32	21
350.....	0.017	0.32	21
375.....	0.013	0.32	21
400.....	0.010	0.32	21
425.....	0.0080	0.33	21
450.....	0.0063	0.33	21
500.....	0.0040	0.33	21
550.....	0.0026	0.33	21
600.....	0.0017	0.33	21
650.....	0.0012	0.33	21

[a] These numbers are appropriate only for rapidly star-forming galaxies similar to those in the sample of § 2.1. The dust SEDs of more typical star-forming galaxies (such as the Milky Way) are significantly different.

strong enough among rapidly star-forming galaxies to substantially reduce the scatter in $\mathscr{K}$ (i.e., to substantially improve estimates of $L_{\rm bol,dust}$ derived from photometry in a single sub-mm window). Illustrating this point, Figure 3 shows $\mathscr{K}(200\ \mu{\rm m})$ ($\equiv L_{\rm bol,dust}/\lambda l_\lambda$ at $\lambda = 200\ \mu$m) versus $L_{\rm bol,dust}$ for each galaxy in our sample. Although LIRGs clearly have systematically different $\mathscr{K}(200\ \mu{\rm m})$ values than ULIRGs, the trend disappears at lower luminosities. Including an absolute luminosity dependence in $\mathscr{K}(\lambda)$ seems unlikely to significantly improve sub-mm constraints on $L_{\rm bol,dust}$.

Measuring the luminosity of a galaxy in two sub-mm bands instead of only one provides additional information about the shape of the dust SED that could in principle be used to estimate $L_{\rm bol,dust}$ more accurately. Unfortunately, the major sub-mm atmospheric windows at 450 and 850 μm both lie in the Rayleigh-Jeans tail of typical dust SEDs at $z \lesssim 3$. Measuring both 450 and 850 μm fluxes of a galaxy at these redshifts therefore reveals little about the temperature of the cold dust component and almost nothing at all about the possible presence of other dust components at higher temperatures. At larger redshifts measuring both fluxes provides better constraints on the shape of the dust SED, but even then two flux measurements cannot uniquely determine the shape of dust SEDs that typically require more than four free parameters for a reasonable fit. In any case accurate fluxes in more than one sub-mm band are seldom available for the faint high-redshift galaxies that are our primary concern. Obtaining these additional sub-mm fluxes may ultimately prove useful for more accurate estimation of galaxies' bolometric dust luminosities, but we will not consider this possibility further.

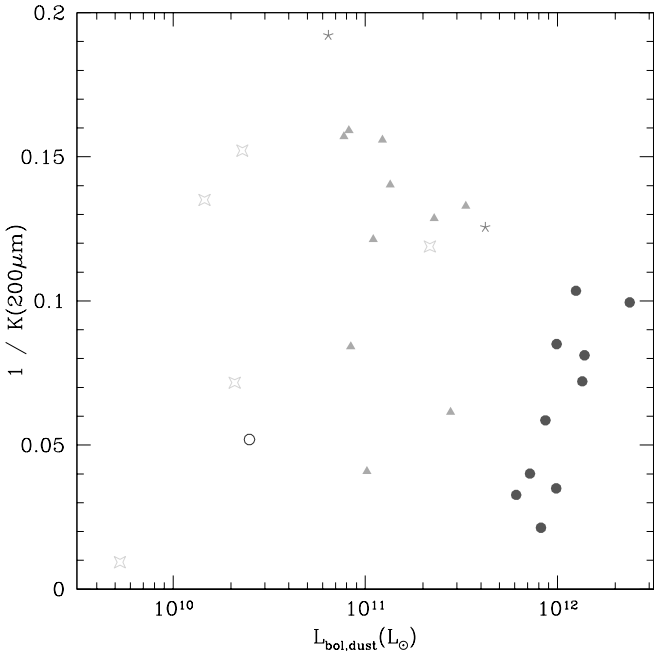

FIG. 3.—Dust SED shapes at different bolometric dust luminosities. The quantity $\mathscr{K}(200\ \mu{\rm m}) \equiv L_{\rm bol,dust}/\nu l_\nu(200\ \mu{\rm m})$ is sensitive to differences in the shapes of galaxies' dust SEDs; its value will be important to us below when we discuss 850 μm fluxes from galaxies at $z \sim 3$. Shown are the values of $1/\mathscr{K}(200\ \mu{\rm m})$ for local galaxies spanning a range of bolometric dust luminosities: ULIRGs (*filled circles*), LIRGs (*triangles*), "interacting galaxies" (*filled stars*), UV-selected starbursts (*open stars*), and M82 (*open circle*). More complete descriptions of these local samples are presented in the text. The bolometric luminosities assume that each galaxy is at a distance of $cz/(75\ {\rm km\ s^{-1}\ Mpc^{-1}})$, except for M82 where we used 3.2 Mpc (Freedman & Madore 1988). Brighter galaxies tend to have hotter dust temperatures and larger values of $\mathscr{K}(200\ \mu{\rm m})$, but this trend has a great deal of scatter and cannot easily be used to improve estimates of galaxies' bolometric dust luminosities derived from observations at $\sim$200 μm rest. See the electronic edition of the Journal for a color version of this figure.

2.2. *Mid-Infrared Constraints on Bolometric Dust Luminosity*

At wavelengths $\lambda \lesssim 15\ \mu$m the dust emission from galaxies tends to rise significantly above the modified blackbody fits discussed in § 2.1. This excess emission is thought to originate from very small grains transiently heated by single UV-photons to high nonequilibrium temperatures; much of it emerges in a few discrete polycyclic aromatic hydrocarbon (PAH) lines at 3.3, 6.2, 7.7, 8.6, and 11.3 μm (see, e.g., Xu et al. 1998 and references therein). 7.7 μm is often the strongest of these lines and the easiest to detect at high redshift. In this subsection we will attempt to quantify the constraints that observations through a 6–9 μm filter can place on a galaxy's bolometric dust luminosity. We will need this information in § 3.3 below.

The sample we will use consists of 11 starbursts and 53 star formation–dominated ULIRGs observed in the mid-IR by Rigopoulou et al. (1999) and the starburst NGC 6090 observed in the mid-IR by Acosta-Pulido et al. (1996).

In analogy to § 2.1 we will define a constant of proportionality $\mathscr{K}_{\rm MIR}$ between bolometric dust luminosity and luminosity at 6 $\mu{\rm m} < \lambda < 9\ \mu$m:

$$L_{\rm bol,dust} = \mathscr{K}_{\rm MIR} \int_{6\mu{\rm m}}^{9\mu{\rm m}} d\lambda l_\lambda\ . \tag{3}$$

After excluding two outliers with anomalously low $\sim 8\ \mu$m luminosities, IRAS 00199−7426 and IRAS 20100−4156, the mean value of $\mathscr{K}_{\rm MIR}$ among the galaxies in this sample is 52, the mean value of $1/\mathscr{K}_{\rm MIR}$ is 0.025, and the rms dispersion in $\log_{10} \mathscr{K}_{\rm MIR}$ is 0.22 dex. Each galaxy's bolometric dust luminosity was estimated from its measured *IRAS* 60 and 100 μm luminosities with the relationship $L_{\rm bol,dust} \simeq 1.47 L_{\rm FIR}$, where $L_{\rm FIR} \equiv 0.65 L_{60} + 0.42 L_{100}$, $L_{60} \equiv \nu l_\nu$ at $\nu = c/60\ \mu$m, and $L_{100} \equiv \nu l_\nu$ at $\nu = c/100\ \mu$m (e.g., Helou et al. 1988). The adopted relationship between $L_{\rm bol,dust}$ and $L_{\rm FIR}$ is satisfied by the galaxies in the sample of § 2.1 with an rms scatter of 7%. The estimated mean and rms of $\mathscr{K}_{\rm MIR}$ are not significantly altered by restricting our analysis either to galaxies with flux measurements in the sub-mm as well as at 60 and 100 μm or to the galaxies with the least noisy mid-IR spectra. Similar values of $\mathscr{K}_{\rm MIR}$ are observed in galaxies with a wide range of bolometric luminosities, as shown in Figure 4.

2.3. *UV Constraints on Bolometric Dust Luminosity*

The methods of estimating $L_{\rm bol,dust}$ discussed so far rely on fitting an average dust SED through the observed dust emission at a single wavelength. $L_{\rm bol,dust}$ can also be estimated without observing any dust emission at all. Many standard methods of estimating the dust content of galaxies rely on the absorption signature of dust in the UV/optical rather than its emission in the far-IR. We will focus our attention on one of these methods, which has been shown (see, e.g., MHC) to predict reasonably well the observed dust emission of local starburst galaxies.

The idea behind this technique is simple. Because dust absorbs shorter wavelengths more strongly than longer

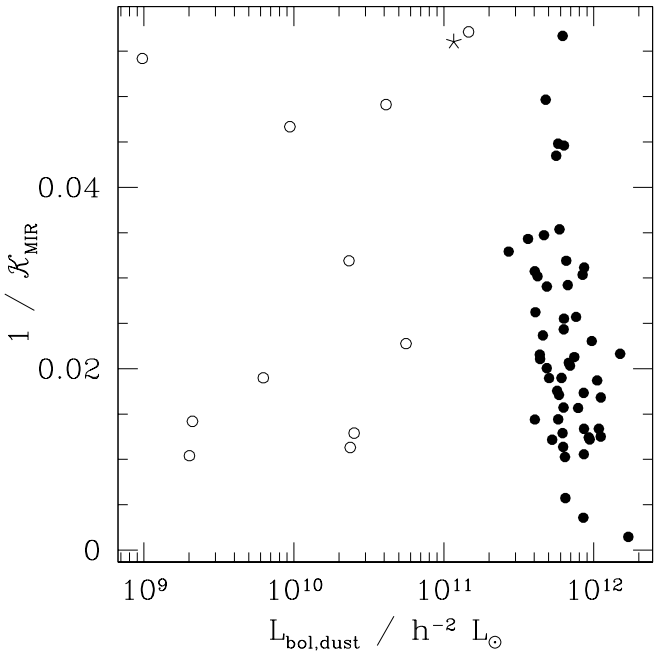

FIG. 4.—Ratio of 6 μm $< \lambda <$ 9 μm PAH luminosity to bolometric dust luminosity ($\mathcal{K}_{MIR} \equiv L_{bol,dust}/\int_{6\ \mu m}^{9\ \mu m} d\lambda l_\lambda$) for rapidly star-forming galaxies in the local universe. Open and solid circles represent starbursts and star formation–dominated ULIRGs observed by Rigopoulou et al. (1999). The star represents the starburst NGC 6090 observed by Acosta-Pulido et al. (1996). Similar values of K_{MIR} are observed in rapidly star-forming galaxies with a large range of bolometric luminosities. See the electronic edition of the Journal for a color version of this figure.

wavelengths, the UV continua of starbursts should become redder on average as the galaxies become dustier and the ratio of far-IR to far-UV luminosity increases. According to MHC, there is surprisingly little scatter in this trend among

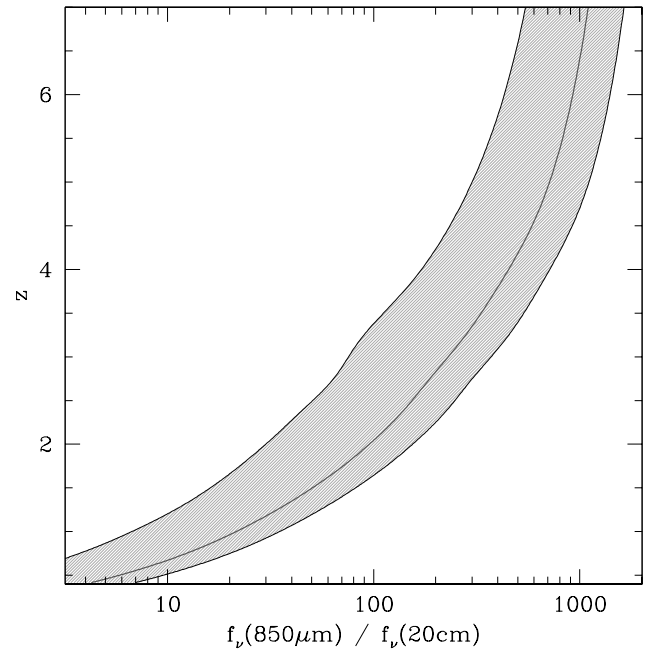

FIG. 5.—Ratio of sub-mm to radio flux as a redshift indicator. The shaded region shows 1 σ limits on the ratio $f_\nu(850\ \mu m)/f_\nu(20\ cm)$ for rapidly star-forming galaxies at different redshifts; the solid line shows the mean ratio. The error bars are skewed for reasons discussed in § 2.4. See also Carilli & Yun (1999, 2000). See the electronic edition of the Journal for a color version of this figure.

starburst galaxies in the local universe; the bolometric dust luminosities of the 57 starburst galaxies in their sample obey

$$L_{bol,dust} = 1.66(10^{0.4(4.43+1.99\beta)} - 1)L_{1600}\ , \qquad (4)$$

where $L_{1600} \equiv \nu l_\nu$ evaluated at $\nu = c/1600$ Å and β is the observed spectral slope ($l_\lambda \propto \lambda^\beta$) at $1200 \lesssim \lambda \lesssim 2000$ Å, with a scatter of 0.3 dex. This correlation is illustrated in Figure 1.

2.4. *Radio Constraints on Bolometric Dust Luminosity*

Observations through the radio atmospheric window can also constrain $L_{bol,dust}$. Increases in far-IR luminosity are accompanied, in local galaxies, by increases in radio emission with a typical spectral slope at $\nu \sim c/20$ cm of $f_\nu \propto \nu^{-0.8}$ (Condon 1992). The radio emission is thought to be synchrotron radiation from electrons in supernova remnants; it is proportional to $L_{bol,dust}$ presumably because supernovae occur in the same population of massive stars responsible for heating the dust. According to Condon (1992), galaxies without active nuclei in the local universe satisfy

$$L_{bol,dust} \simeq 7.9 \times 10^5 L_{20}\ , \qquad (5)$$

where $L_{20} \equiv \nu l_\nu$ at $\nu = c/20$ cm, with a scatter of 0.2 dex. This relationship is usually expressed in terms of the quantity L_{FIR}; the constant of proportionality in equation (5) assumes $L_{bol,dust} \simeq 1.47 L_{FIR}$, as discussed in § 2.2.

The local radio/far-IR relation (eq. [5]) is unlikely to hold to arbitrarily high redshifts. At some redshift the energy density of the cosmic microwave background, increasing as $(1+z)^4$, will become comparable to the magnetic energy density in star-forming galaxies, and relativistic electrons in supernova remnants will begin to cool through inverse Compton scattering rather than synchrotron emission. For magnetic energy densities comparable to those observed among rapidly star-forming galaxies in the local universe, this will occur at $z \gtrsim 3$–6 (e.g., Carilli & Yun 1999).

We conclude this section with a brief digression. Carilli & Yun (1999) have recently proposed the ratio $\eta \equiv f_\nu(850\ \mu m)/f_\nu(20\ cm)$ as a photometric redshift estimator. Results in this section allow us to quantify the estimator's likely accuracy. Equations (2) and (5) imply

$$\eta \simeq \frac{3400(1+z)^{-1-\alpha}}{\mathcal{K}(850\mu m/1+z)}\ , \qquad (6)$$

where $\alpha \simeq -0.8$ is the spectral index of the radio emission and $\mathcal{K}(\lambda)$ can be interpolated from Table 1. Calculating the mean expected η and its uncertainty as a function of redshift is complicated by the logarithmic uncertainties and by the presence of $\mathcal{K}$ in the denominator of equation (6). To calculate the mean expected value of η we used $\bar{\eta} = 3400(1+z)^{-\alpha-1}\langle 1/\mathcal{K}(850\ \mu m/1+z)\rangle$, where $\langle 1/\mathcal{K}\rangle$ is the mean value of $1/\mathcal{K}$ among the galaxies in § 2.1; to calculate the (asymmetrical) 1 σ uncertainties in η we assumed that $\log_{10}(\eta)$ was symmetrically distributed around $\mu \equiv \log_{10}(\bar{\eta}) - \sigma_{dex}^2 \log_e 10/2$, where σ_{dex}, the logarithmic spread in η for galaxies at a given redshift, is the quadrature sum of the logarithmic uncertainty in $\mathcal{K}(\lambda)$ (from Table 1) and the 0.2 dex scatter in the radio/far-IR correlation. If the uncertainty in $\log_{10}(\eta)$ has a Gaussian distribution—as is roughly the case—this choice of μ correctly reproduces the desired mean $\bar{\eta}$. We will handle denominator terms and

logarithmic uncertainties similarly throughout this paper unless stated otherwise.

Figure 5 shows the expected range of η for star-forming galaxies as a function of redshift; redshift has been placed on the ordinate to allow redshift constraints to be easily read off this figure given a measured value of η. This figure can be used to estimate redshifts of a star-forming galaxies on the basis of their 850 μm and 20 cm fluxes, but the estimates will be accurate only if these galaxies obey the local radio to far-IR correlation (eq. [5]) and have similar dust SEDs as the local sample of § 2.1. Our next section is concerned, in part, with whether this is true (see also Carilli & Yun 2000).

3. OBSERVATIONS AT HIGH REDSHIFT

With very few exceptions, galaxies at high redshift are too faint to have been detected over the wavelength range 20 $\mu\mathrm{m} \lesssim \lambda \lesssim 200$ μm by any satellite that has flown. Their bolometric dust luminosities therefore cannot be directly measured; they can only be indirectly estimated with the correlations we have just described between $L_{\mathrm{bol,dust}}$ and luminosities at accessible wavelengths. Unfortunately, the underlying physics responsible for these empirical correlations is poorly understood, and so there is no particular theoretical reason to expect them to exist in identical form at high-redshift. Nor can their existence be directly established empirically, for without measuring high-redshift galaxies' fluxes at several wavelengths 20 $\mu\mathrm{m} \lesssim \lambda \lesssim 200$ μm it is impossible to show directly that their bolometric dust luminosities are correlated in the expected way with their fluxes through various atmospheric windows. It might therefore appear that the assumptions required to estimate high-redshift galaxies' bolometric dust luminosities (and therefore star formation rates) are not only questionable but also untestable; but this is not entirely true. If a galaxy's fluxes in the rest-UV, mid-IR, sub-mm, and radio are each correlated with its bolometric dust luminosity, then they should also be correlated with each other in a way that is straightforward to calculate. Observing high-redshift galaxies at more than one of these wavelengths therefore provides an indirect test of standard methods for estimating $L_{\mathrm{bol,dust}}$. These indirect tests are the subject of this section.

Because our ultimate goal is to estimate the 850 μm fluxes of known UV-selected high-redshift populations from their UV colors, our emphasis in this section will be on testing whether high-redshift galaxies have the mid-IR, sub-mm, and radio fluxes that their UV-colors and the correlations in § 2 would predict. This should not give the false impression that we are testing solely whether MHC's β/far-IR relation is satisfied by high-redshift galaxies. Without directly measured bolometric dust luminosities, it is impossible to test for the existence of any one of the correlations of § 2 independently of the others; they can only be tested in pairs. If $z \sim 3$ galaxies are found to have radio fluxes at odds with our predictions from their far-UV properties, for example, it might mean that they do not obey the local β/far-IR relation, but it could equally well mean that they do not obey the local radio/far-IR relation. What we are really testing in this section is whether high-redshift star-forming galaxies are sufficiently similar to their low-redshift counterparts for their bolometric dust luminosities and star formation rates to be reliably estimated in the absence of complete photometry at rest wavelengths 20 $\mu\mathrm{m} \lesssim \lambda \lesssim 200$ μm.

The observations required for these tests are extremely difficult with current technology, and even though the data analyzed in this section are among the best available, much of the evidence presented is rather marginal. We have included even inconclusive evidence below when it illustrates what can (and cannot) be learned from currently feasible observations.

3.1. *SMM J14011*

The lensed galaxy SMM J14011+0252 at $\alpha(\mathrm{J2000}) = 14^{\mathrm{h}}01^{\mathrm{m}}04^{\mathrm{s}}.97$, $\delta(\mathrm{J2000}) = +02^{\circ}52'24''.6$, $z = 2.565$ (Smail et al. 1998; Frayer et al. 1999) is the only sub-mm–selected object robustly confirmed to be a high-redshift galaxy without an obviously active nucleus (e.g., Ivison et al. 2000). 450 μm, 850 μm, and 20 cm fluxes for this object were obtained by Ivison et al. (2000). We obtained rest-UV photometry through the G and $\mathscr{R}$ filters (Steidel & Hamilton 1993) with COSMIC (Kells et al. 1998) on the Palomar 200 inch Hale telescope in 1999 March. Our optical photometry of SMM J14011 is presented in Table 2.

Predicting SMM J14011's radio and sub-mm fluxes from its UV photometry requires an estimate of the slope of its UV continuum, β (in $f_\lambda \propto \lambda^\beta$; see § 2.3). Estimating β from UV photometry is not entirely trivial for two reasons. First, the observed UV continua of high-redshift galaxies have been reddened by the intergalactic absorption of the Lyα forest, and this must be corrected before we can estimate their intrinsic continuum slopes β. Second, the UV continua of starburst galaxies are not exactly power laws, and so fitting their continua over different wavelength ranges can produce different estimates of the best-fit slope β. MHC calculated β for galaxies in their local sample by fitting these galaxies' fluxes through 10 "windows" spanning the wavelength range $1260\text{Å} < \lambda < 2600\text{Å}$; nine of these windows were bluer than 1950 Å. The available photometry of high-redshift galaxies rarely covers an identical wavelength range. At SMM J14011's redshift of $z = 2.565$, for example, the G and $\mathscr{R}$ filters sample $\sim$1350 and $\sim$1950 Å rest. To estimate β for SMM J14011 in a way that took some account of these complications, we first subjected a GISSEL96 model of an actively star-forming galaxy (A. Bruzual & S. Charlot 1996, private communication) to the appropriate intergalactic absorption (Madau 1995) and

TABLE 2

PHOTOMETRY

Object	G^{a}	R^{a}	i^{a}	J^{b}	H^{b}	K_s^{b}
SMM J14011[c]	21.94	21.25	...	19.33	18.44	17.69
West MMD11.....	25.09	24.05	23.84	21.28	20.12	19.44

[a] AB system.
[b] Vega system.
[c] Sum of the components J1 and J2.

then reddened the resulting spectrum with increasing dust extinction following a Calzetti (1997) law until this synthetic spectrum had the same G and $\mathscr{R}$ colors as SMM J14011. Finally, we fitted this synthetic spectrum through the 10 windows of MHC with a power-law of the form $l_\lambda \propto \lambda^\beta$. The best-fit β we find—which is rather insensitive to the details of this procedure—is $\beta = -0.74$, with a 1 σ uncertainty due to photometric errors of ± 0.25.

Equations (2)–(4) can now be used to predict SMM J14011's radio and sub-mm fluxes from its UV photometry. Defining the constants

$$\mathscr{K}_{850}(z) \equiv L_{\rm bol,dust}/\nu l_\nu \quad \text{at} \quad \nu = c(1+z)/850\ \mu\text{m}\ , \tag{7a}$$

$$\mathscr{K}_{450}(z) \equiv L_{\rm bol,dust}/\nu l_\nu \quad \text{at} \quad \nu = c(1+z)/450\ \mu\text{m}\ , \tag{7b}$$

$$\mathscr{K}_L(z,\alpha) \equiv L_{\rm bol,dust}/\nu l_\nu \simeq 7.9\times 10^5 (1+z)^{-(1+\alpha)} \quad \text{at} \quad \nu = c(1+z)/20\ \text{cm}\ , \tag{7c}$$

and

$$\mathscr{K}_{\mathscr{R}}(z,\beta) \equiv L_{1600}/\nu l_\nu \simeq (4.3/1+z)^{\beta+1} \quad \text{at} \quad \nu = c(1+z)/6900\ \text{Å}\ , \tag{7d}$$

where $\alpha \simeq -0.85 \pm 0.16$ (Richards 2000) is the slope of the synchrotron emission (in $f_\nu \propto \nu^\alpha$), β is the slope of the UV-continuum, as defined above, and 6900 Å is approximately the central wavelength of the $\mathscr{R}$ filter, and using $f_\nu = 10^{-0.4(m_{\rm AB}+48.60)}$ ergs s^{-1} cm^{-2} Hz^{-1}, we find, after substituting into equations (2), (4), and (5), and changing from l_ν to f_ν with the equation $l_{\nu_1}/l_{\nu_2} = f_{\nu_1}/f_{\nu_2}$, the following relationships between the observed-frame optical, sub-mm, and radio fluxes of star-forming galaxies at $z \sim 3$:

$$f_{\nu,\rm obs}(850\ \mu\text{m}) \sim 10^{-0.4(\mathscr{R}-22.17)}\left[\frac{\mathscr{K}_{\mathscr{R}}(z,\beta)}{1.}\right]\left[\frac{\mathscr{K}_{850}(z)}{10.}\right]^{-1} \times (10^{0.4(4.43+1.99\beta)}-1)\ \text{mJy}\ , \tag{8}$$

$$f_{\nu,\rm obs}(450\ \mu\text{m}) \sim 10^{-0.4(\mathscr{R}-22.98)}\left[\frac{\mathscr{K}_{\mathscr{R}}(z,\beta)}{1.}\right]\left[\frac{\mathscr{K}_{450}(z)}{2.5}\right]^{-1} \times (10^{0.4(4.43+1.99\beta)}-1)\ \text{mJy}\ , \tag{9}$$

$$f_{\nu,\rm obs}(1.4\ \text{GHz}) \sim 10^{-0.4(\mathscr{R}-23.86)}\left[\frac{\mathscr{K}_{\mathscr{R}}(z,\beta)}{1.}\right] \times \left[\frac{\mathscr{K}_L(z,\alpha)}{6.0\times 10^5}\right]^{-1}(10^{0.4(4.43+1.99\beta)}-1)\ \mu\text{Jy}\ , \tag{10}$$

with no dependence on cosmology. The redshift dependence is contained in the K-corrections $\mathscr{K}_{450}$, $\mathscr{K}_{850}$, $\mathscr{K}_{\mathscr{R}}$, and $\mathscr{K}_L$; the default values of $\mathscr{K}_{850} = 10$, $\mathscr{K}_{450} = 2.5$, $\mathscr{K}_{\mathscr{R}} = 1$, $\mathscr{K}_L = 6.0\times 10^5$ in this equation, derived from equations (7a)–(7d) and Table 1, are roughly appropriate for $z \simeq 3.0$. The uncertainty in these equations is large. Equation (4) is able to predict $L_{\rm bol,dust}$ from starbursts' UV luminosities and spectral slopes with an uncertainty of about 0.3 dex. At fixed $L_{\rm bol,dust}$ there is (as argued in § 2.1) an additional uncertainty of 0.1 dex in l_ν at 100 μm $\simeq$ 450 μm/1 + z, 0.3 dex at 200 μm $\simeq$ 850 μm/1 + z, and 0.2 dex at 6 cm $\simeq$ 20 cm/1 + z. If these logarithmic uncertainties add in quadrature, we would expect equations (8), (9), and (10) to be able to predict sub-mm and radio fluxes from UV fluxes to within 0.3–0.4 dex, if high-redshift galaxies resembled local starbursts exactly.

For a galaxy at $z = 2.565$ with $\beta = -0.74$, the appropriate K-correction constants for equations (8)–(10) are $\mathscr{K}_{\mathscr{R}} = 1.05$, $\mathscr{K}_L = 6.13\times 10^5$, and, interpolating between the values listed in Table 1, $\mathscr{K}_{850} = 15.3$ and $\mathscr{K}_{450} = 2.6$. These equations then predict 850 μm, 450 μm, and 20 cm fluxes for SMM J14011 of 23^{+14}_{-9} mJy, 70^{+43}_{-28} mJy, 150^{+95}_{-67} μJy. The quoted uncertainties reflect only the uncertainty in β from photometric errors. An additional uncertainty of $\sim$0.4 dex applies to each predicted flux, and so these predicted fluxes agree well with the measured fluxes (Ivison et al. 2000) $f_\nu(850\ \mu\text{m}) = 15 \pm 2$ mJy, $f_\nu(450\ \mu\text{m}) = 42 \pm 7$ mJy, $f_\nu(20\ \text{cm}) = 115 \pm 30$ μJy (see Fig. 6). SMM J14011 evidently exhibits the same relationship between its UV, far-IR, and radio properties as rapidly star-forming galaxies in the local universe.

3.2. *Lyman-Break Galaxies*

3.2.1. *Sub-mm*

Although it is encouraging that one galaxy at $z \sim 3$, SMM J14011+0252, appears similar to local galaxies in the correlations of its rest-frame UV, sub-mm, and radio fluxes, ideally we would like to establish that this holds true for entire populations of galaxies at $z \sim 3$. Unfortunately, this is exceedingly difficult with current technology. None of the $\sim$800 spectroscopically confirmed $z \sim 3$ galaxies in the UV-selected sample of Steidel et al. (2000, in preparation), for example, has an $\mathscr{R}$ magnitude as bright as SMM J14011's $\mathscr{R} = 21.25$, and $\sim$95% of the galaxies in that sample are more than 10 times fainter. Even if these galaxies were as heavily obscured as SMM J14011, we would expect their 850 μm fluxes to be at least 10 times lower than SMM J14011's, or $\lesssim$1 mJy, well below SCUBA's detection limit. (SCUBA, on the James Clerk Maxwell Telescope, is the current state-of-the-art sub-mm bolometer array; see Holland et al. 1999). This suggests that (typical) individual Lyman-break galaxies are unlikely to be detected with SCUBA, and tests of whether these galaxies have the bolometric dust luminosities predicted from their UV spectral slopes will be at best statistical.

The faintness of typical Lyman-break galaxies makes their sub-mm and radio fluxes difficult to predict as well. Predicted bolometric dust luminosities depend sensitively

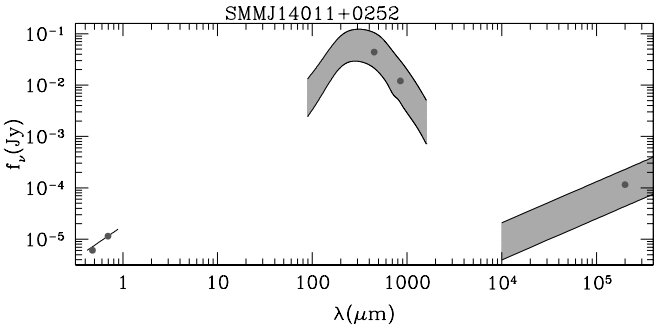

FIG. 6.—Optical to radio SED of the lensed star-forming galaxy SMM J14011+0252 at $z = 2.565$. Circles show measured fluxes (see text for references). G and $\mathscr{R}$ photometry were used to estimate the slope of this galaxy's (rest) far-UV continuum (*solid line*). This slope was then used to predict the far-IR and radio properties of SMM J14011 as described in §§ 2 and 3.1. The measured sub-mm and radio fluxes fall within the ± 1 σ predicted region (*shaded*), suggesting that SMM J14011 follows the same relation between its UV, far-IR, and radio properties as local starburst galaxies. See the electronic edition of the Journal for a color version of this figure.

on the UV spectral slope β, and this slope is difficult to estimate accurately for faint objects with relatively large photometric errors. For example, if a galaxy at $z = 2.6$ had $G - \mathscr{R} = 0.75$, we would estimate (using the method of § 3.1) $\beta = -0.60$ and $L_{\rm bol,dust} \simeq 31 \times L_{1600}$, while if it had $G - \mathscr{R} = 0.95$ we would estimate $\beta = -0.07$ and $L_{\rm bol,dust} = 85 \times L_{1600}$. A photometric error of 0.2 in $G - \mathscr{R}$ is not unusual for Lyman-break galaxies, especially at fainter magnitudes (e.g., Adelberger et al. 2000, in preparation), and so photometric errors can easily affect our predicted sub-mm and radio fluxes by a factor of ~ 3.

The situation is worsened by the fact that the only Lyman-break galaxies likely to be detectable in the sub-mm or radio are those with reddest UV slopes and highest dust obscurations. Subsamples of Lyman-break galaxies selected for follow-up observations at these wavelengths will have to be chosen from among the reddest members of the population. Because highly reddened Lyman-break galaxies are much rarer than their less reddened counterparts (cf. Fig. 12, discussed below), and because the typical photometric errors on Lyman-break galaxies are large, there is a reasonable chance that a Lyman-break galaxy which appears to be heavily reddened is actually a less reddened galaxy with photometric errors. These subsamples will therefore suffer from significant Malmquist bias.

For these reasons, observing Lyman-break galaxies in the sub-mm does not appear to be an especially promising way to test whether these galaxies obey the β/far-IR correlation. Nevertheless, Chapman et al. (2000) have attempted the observations. Their results are shown in Figure 7.

In order to calculate predicted sub-mm fluxes for these galaxies in a way that accounted for the significant photometric uncertainty and Malmquist bias discussed above, and for the expected intrinsic scatter in the UV/850 μm relationship (eq. [8]), we proceeded as follows. We first generated a large ensemble of simulated Lyman-break galaxies with $\mathscr{R}$ magnitudes drawn at random from the $z \sim 3$ LBG luminosity function shown in Figure 12, UV slopes β drawn at random from the distribution in Figure 12 (cf. Steidel et al. 1999; Adelberger et al. 2000, in preparation), and redshift z drawn at random from the interval $2.5 < z < 3.5$. Each of these galaxies was assigned a G magnitude by inverting the procedure of § 3.1, and an 850 μm flux using equation (8). The 850 μm fluxes were then changed randomly to reflect the scatter in the β/far-IR relation and in $\mathscr{K}_{850}(z)$. Finally, we placed each simulated galaxy at a random location in our G and $\mathscr{R}$ images and attempted to detect it and measure its photometry with the same software used to find real Lyman-break galaxies in these images. This produced a long list of the $\mathscr{R}$ magnitudes and $G - \mathscr{R}$ colors we would expect to measure for Lyman-break galaxies with known redshifts and 850 μm fluxes if the galaxies obeyed the local β/far-IR relation and had dust SEDs similar their local analogs. In order to predict the 850 μm fluxes shown in Figure 7, we binned together the 850 μm fluxes of simulated galaxies with magnitudes, colors, and redshifts similar to those of each galaxy in the sample of Chapman et al. (2000). As our best guess of the predicted 850 μm flux for each galaxy in the Chapman et al. sample, we took the sample mean of the 850 μm flux among simulated galaxies in its bin; for the uncertainty in the predicted flux we took the standard deviation of the 850 μm fluxes of these same simulated galaxies.

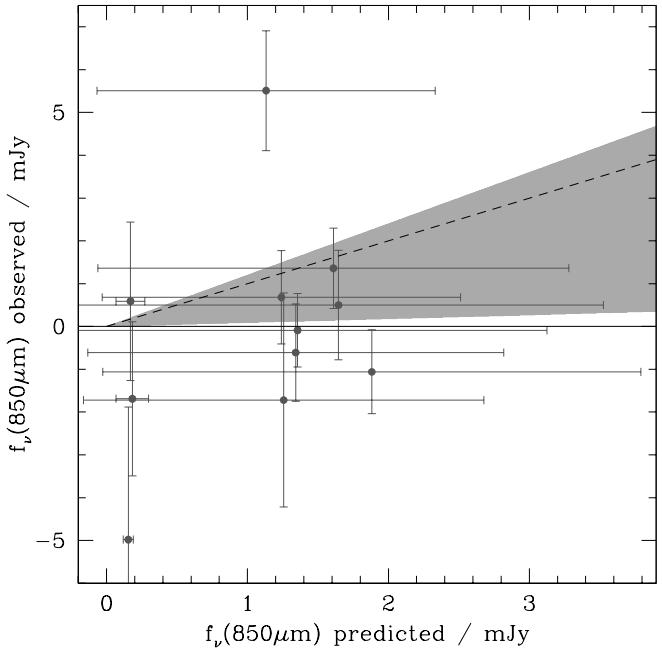

FIG. 7.—Predicted and observed 850 μm fluxes of 11 LBGs observed by Chapman et al. (2000). The shaded region shows the 90% credible interval on the slope of the line $f_{850,\rm observed} = b \times f_{850,\rm predicted}$. The large error bars on the predicted fluxes, which arise for reasons discussed in § 3.2, are plotted symmetrically about the mean for simplicity, though in fact they are very skewed. Monte Carlo simulations suggest that most Lyman-break galaxies will have observed fluxes smaller than the predicted mean and that a small fraction will have observed fluxes significantly larger. See the electronic edition of the Journal for a color version of this figure.

For simplicity we have indicated in Figure 7 the uncertainties in the predicted fluxes with the convention mean $\pm$ rms, but in fact these uncertainties are very skewed. The Monte Carlo simulations just described suggest that most Lyman-break galaxies should have 850 μm fluxes lower than the mean value and that some will have 850 μm fluxes significantly larger (how else could we have mean $\sim$rms with the predicted fluxes bounded below by zero?), and so the observations are more consistent with the predictions than Figure 7 might suggest at first glance.

One way to quantify the agreement of the observations with our predictions is to calculate χ^2. Denoting the predicted fluxes by x and the observed by y, the relevant χ^2 figure of merit,

$$\chi^2 \equiv \sum_{i=1}^{N} \frac{(x_i - y_i)^2}{\sigma_{x,i}^2 + \sigma_{y,i}^2} \qquad (11)$$

(e.g., Press et al. 1992, § 15.3) is equal to 14.5. There are 11 data points and no free parameters in this fit, and so the data are at least not grossly inconsistent with our expectations. It is difficult to make a more quantitative statement with this approach, however, because the error bars on the predicted flux are very skewed, and χ^2 is therefore not drawn from the usual distribution derived for Gaussian uncertainties.

An alternate approach is to ask what these data say about slope b of the line $f_{\rm observed} = b f_{\rm predicted}$. If Lyman-break galaxies obeyed the β/far-IR correlation and had dust SEDs similar to those of local galaxies, we would expect the data to be consistent with $b = 1$. A Bayesian approach can quantify the constraints on b in a way that takes proper account of our skewed uncertainties. This approach

requires us to calculate the likelihood of the data as a function of b. In the brief derivation below, f_m and σ denote measured 850 μm fluxes and uncertainties for the galaxies in Chapman et al. (2000), f_t denotes these galaxies' (unknown) true fluxes that would be measured if we had perfect data, $f'_t \equiv f_t/b$ denotes the true 850 μm fluxes of the *simulated* Lyman-break galaxies, calculated above under the assumption $b = 1$, and I is shorthand for the background knowledge (such as the luminosity and β distributions of Lyman-break galaxies, and the scatter in the β/far-IR relation, and so on) that went into our Monte Carlo simulations. Our data set consists of the redshifts $\{z\}$, apparent magnitudes $\{\mathscr{R}\}$, colors $\{G-\mathscr{R}\}$, and 850 μm fluxes $\{f_m\}$ of each galaxy the sample of Chapman et al. (2000). The likelihood of observing these data given b is equal to the product of the likelihoods of observing each galaxy individually:

$$P(\{G-\mathscr{R}\}\{\mathscr{R}\}\{z\}\{f_m\}\,|\,\{\sigma\}bI) = \prod_i^N P[(G-\mathscr{R})_i \mathscr{R}_i z_i\, f_{m,i}\,|\,\sigma_i bI]\ . \quad (12)$$

These individual likelihoods can be evaluated by integrating over the unknown true 850 μm flux of each galaxy:

$$P[(G-\mathscr{R})\mathscr{R}z f_m\,|\,\sigma bI] = \int_0^\infty df_t\, P(f_t\,|\,bI) \times P[(G-\mathscr{R})\mathscr{R}z\,|\,f_t I]P(f_m\ |\,f_t\sigma)\ . \quad (13)$$

We have simplified this equation by omitting irrelevant variables from the conditional probabilities and by writing $P(AB)$ as $P(A)P(B)$ when A and B are independent. $P(f_m|f_t\sigma)$ can be calculated by assuming that the uncertainties in the measured fluxes are Gaussian, which is roughly true. The remaining probabilities in the integral can be estimated from the Monte Carlo simulations. Writing the total number of galaxies in the simulations as $N_{\rm tot}$, and the number of galaxies in the simulations with both properties A and B as $n(A, B)$, we have $P(f_t\,|\,bI) \simeq n(f'_t)/N_{\rm tot}$ and $P[(G-\mathscr{R})\mathscr{R}z\,|\,f_t I] \simeq n(G-\mathscr{R}, \mathscr{R}, z, f'_t)/n(f'_t)$. Substituting into equation (12) yields the likelihood, given b, of observing a single galaxy at redshift z with UV photometry $\mathscr{R}$ and $G-\mathscr{R}$ and 850 μm flux f_m:

$$P[(G-\mathscr{R})\mathscr{R}z f_m\,|\,\sigma bI] \propto \int_0^\infty df'_t\, n(G-\mathscr{R}, \mathscr{R}, z, f'_t) \times \exp\left[-\frac{1}{2}\left(\frac{bf'_t - f_m}{\sigma}\right)^2\right]. \quad (14)$$

The maximum likelihood value of b, calculated numerically using equations (12) and (14), is $b = 0.45$. For a uniform prior, the 68% and 90% highest posterior density regions are $0.22 \le b \le 0.87$ and $0.09 \le b \le 1.2$. The sub-mm fluxes of Lyman-break galaxies therefore appear to be somewhat lower than we would have expected. This could indicate that Lyman-break galaxies do not quite satisfy MHC's β/far-IR correlation, or that their dust SEDs are different from those of the local galaxies described in § 2.1; but the inconsistency with $b = 1$ is only marginally significant and we will not speculate further about its possible cause. All we can say with much confidence is that the sub-mm fluxes of Lyman-break galaxies are unlikely to be either much higher or more than an order of magnitude lower than our predictions.

Our interpretation of these data differs quantitatively from that of Chapman et al. (2000). This is because those authors ignored the uncertainties in the predicted fluxes in most of their analysis, and assumed that the dust SEDs of all Lyman-break galaxies would be well approximated by a single modified blackbody (eq. [1]) with $T = 50$ K and $\epsilon = 1.5$, rather than by the range of empirical SEDs estimated in § 2.1.

3.2.2. *Radio*

Radio observations of Lyman-break galaxies can in principle provide another indirect test of standard methods for estimating these galaxies' bolometric dust luminosities. Extremely deep radio images are required, however, if we hope to put interesting limits on the radio fluxes of typical $z \sim 3$ galaxies: equation (10) implies that the vast majority of Lyman-break galaxies in the sample of Steidel et al. (2000, in preparation) will have 20 cm fluxes of only a few μJy or less. One of the deepest existing radio images is Richards's (2000) 20 cm VLA map of the Hubble Deep and Flanking Fields, which reaches a 1 σ noise limit of 8 μJy beam^{-1}. Unfortunately, even this image does not appear sufficient for a meaningful test. Of the 46 Lyman-break galaxies in our spectroscopic sample that lie within this 20 cm image, only two are predicted (using the Monte Carlo method of § 3.2.1) to have marginally detectable fluxes $f_\nu > 10$ μJy. These two, with predicted fluxes of 12 ± 15 and 19 ± 17 μJy, have observed fluxes of 4 ± 12 and -6 ± 12 μJy—not exactly in line with our predictions, but not damning either. (Our method of estimating the observed fluxes is described in § 3.3.2 below.) Nine galaxies have marginally significant observed fluxes of $f_\nu > 10$ μJy, and none of these nine were predicted to be especially bright; but six galaxies have measured fluxes $f_\nu < -10$ μJy, and so even the marginally significant detections may simply reflect the noise characteristics of Richards's (2000) image. Statistical tests based on the sample as a whole are as inconclusive as the object-by-object tests we have just described: the total observed and predicted 20 cm fluxes from these 46 galaxies are 105 ± 81 and 114 ± 36 μJy, respectively, and the formal 90% credible interval on $b \equiv f_{\rm observed}/f_{\rm predicted}$, estimated using the Monte Carlo simulations and Bayesian approach of § 3.2.1, is $0 < b < 2.1$.

3.3. *Balmer-Break Galaxies*

Galaxies at redshifts as high as $z \sim 3$ are hardly ideal for testing whether the UV-properties of high-redshift galaxies can be used to predict their bolometric dust luminosities, because large luminosity distances and unfavorable K-corrections make them extremely faint in the optical, mid-IR, and radio (cf. Fig. 1). A better redshift is $z \sim 1$. At this redshift galaxies are much brighter in these atmospheric windows, and their far-UV spectral slopes β can still be measured with ground-based photometry. In this section we will use galaxies drawn from the $z \sim 1$ "Balmer-break" sample of Adelberger et al. (2000, in preparation) to test whether actively star-forming galaxies at $z \sim 1$ follow the correlations between UV, mid-IR, and radio properties observed among galaxies in the local universe. This color-selected sample consists of $\sim$700 star-forming galaxies with spectroscopic redshifts $0.9 \lesssim z \lesssim 1.1$ and apparent magnitudes $\mathscr{R} \lesssim 25.5$.

One warning is due before we begin. The β/far-IR correlation of MHC (eq. [4]) has been shown to hold only for

starburst galaxies in the local universe. It is not known whether less rapidly star-forming galaxies such as the Milky Way satisfy this correlation, and poststarburst galaxies, whose red UV slopes reflect age rather than dust content, almost certainly do not. At $z \sim 3$ galaxies are bright enough to satisfy the Lyman-break criteria of Steidel et al. (1999) only if they are forming stars rapidly ($\gtrsim 30\ M_\odot\ \mathrm{yr}^{-1}$ with typical dust obscurations, for $h = 0.7$, $\Omega_M = 0.3$, $\Omega_\Lambda = 0.7$), and so these galaxies might reasonably be expected to obey the β/far-IR correlation (see MHC for further discussion of the Lyman-break galaxy/starburst connection). But at $z \sim 1$ poststarburst galaxies and slowly star-forming galaxies like the Milky Way can both satisfy our Balmer-break selection criteria, in addition to the starburst galaxies that are expected to obey the β/far-IR correlation. There is therefore good reason to suspect a priori that some galaxies in our Balmer-break sample will not obey this correlation.

In principle one might be able to select the starburst analogs from among a Balmer-break sample on the basis of their photometric or spectroscopic signatures, but a proper treatment is beyond the scope of this paper. Fortunately, slowly star-forming galaxies will be far too faint in the radio and mid-IR to be detected in current data, and so their presence in our Balmer-break sample will not significantly affect the conclusions of this subsection. A crude way of partially excluding poststarbursts, which we shall adopt below, is to impose an additional selection criterion $U_n - G < 0.5$ on the Balmer-break sample. This limits the Balmer-break sample to the same range of β observed among starburst galaxies in the local universe and among Lyman-break galaxies at $z \sim 3$ by excluding the galaxies that are reddest in the far-UV, whose slopes might reflect age rather than their dust content. We will discuss this further elsewhere (Adelberger et al. 2000, in preparation).

3.3.1. *Mid-Infrared*

Because of the strength of the 7.7 μm PAH feature, 15 μm observations provide a particularly promising way of observing dust emission from galaxies at $z \sim 1$. Seventy-one Balmer-break galaxies from our spectroscopic sample lie within the 15 μm (LW3) ISO image of the CFRS 1415+52 field obtained by Flores et al. (1999); six of them are listed as optical counterparts to 15 μm sources in these authors' 3 σ catalog.

Equations (3) and (4) imply the following relationship between the UV and mid-IR photometry of galaxies at $z \sim 1$:

$$f_{\nu,\mathrm{obs}}(15\ \mu\mathrm{m}) \sim 10^{-0.4(U_n - 25.22)} \left[\frac{\mathscr{K}_U(z,\beta)}{1}\right] \left(\frac{\mathscr{K}_{15}}{20}\right)^{-1} \times (10^{0.4(4.43+1.99\beta)} - 1)\ \mu\mathrm{Jy}\ , \quad (15)$$

where

$$\mathscr{K}_{15} \equiv L_{\mathrm{bol,dust}}/\nu \bar{l}_\nu \quad \text{at} \quad \nu = c(1+z)/15\ \mu\mathrm{m}\ , \quad (16)$$

$$\mathscr{K}_U(z,\beta) \equiv L_{1600}/\nu l_\nu \simeq \left(\frac{1+z}{2.3}\right)^{\beta+1} \quad \text{at} \quad \nu = c(1+z)/3700\ \text{Å}\ , \quad (17)$$

$\bar{l}_\nu$ is the mean luminosity density at rest frequencies $c(1+z)/18\ \mu\mathrm{m} < \nu < c(1+z)/12\ \mu$m, and 3700 Å is roughly the central wavelength of the U_n filter after accounting for atmospheric absorption and instrumental throughput. In most cases the observed 15 μm fluxes of $z \sim 1$ galaxies are dominated by emission from the 7.7 and 8.6 μm PAH lines, and $\mathscr{K}_{15}$ depends very weakly on redshift near $z \sim 1$. It is well approximated by $\mathscr{K}_{\mathrm{MIR}}/2.4 \simeq 22$ for all the redshifts we will consider here ($\mathscr{K}_{\mathrm{MIR}}$ is defined in § 2.2).

To estimate β for these galaxies we used their $U_n - G$ colors, which sample rest wavelengths $\sim$1850 and $\sim$2350 Å, and a procedure analogous to the one described in § 3.1. Photometric errors are less of a concern for these optically bright galaxies than for the faint $z \sim 3$ galaxies of § 3.2. Instead of taking the elaborate Monte Carlo approach of § 3.2, we estimated the predicted 15 μm fluxes for these galaxies by assuming that their true U_n magnitudes and $U_n - G$ colors were equal on average to the measured values; for the uncertainty in the predicted fluxes we simply propagated through the uncertainties in the $U_n - G$ and U_n fluxes determined from the Monte Carlo simulations. The total uncertainty in the predicted fluxes, 0.5 dex, arises from the scatter in the β/far-IR correlation (0.3 dex), from the expected scatter in $\mathscr{K}_{15}$ (0.2 dex), from photometric uncertainties in U_n magnitudes (0.1 dex), and from the uncertainty in β due to photometric errors in $U_n - G$ (0.3 dex).

Figure 8 shows the predicted and observed 15 μm fluxes of these 71 Balmer-break galaxies. The majority of these galaxies do not appear in the 3 σ catalog of Flores et al. (1999), and so we know only that their fluxes were less than $\sim$150 μJy; these sources are indicated with downward pointing arrows. The detections are indicated by points with error bars.

These data appear encouragingly consistent with our UV-based predictions: the large number of galaxies with predicted flux significantly lower than the detection limit are not detected, while the majority of those with predicted fluxes close to (or above) the detection limit are. The only apparently serious discrepancy between predicted and observed fluxes (ISO 138 with $f_{\mathrm{predicted}} \sim 4$, $f_{\mathrm{observed}} \sim 250$), may result from a misidentification of the optical galaxy responsible for the 15 μm emission; according to Flores et al. (1999) there is a 27% chance of misidentification for this object, compared to a median 3% chance for the other five detections.

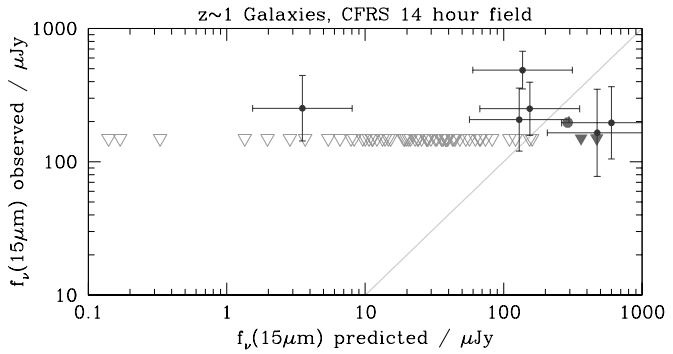

FIG. 8.—Predicted and observed 15 μm fluxes of Balmer-break galaxies at $z \sim 1$. The majority of these galaxies are undetected at a 3 σ limit of 150 μJy; uncertainties on the predicted fluxes of these galaxies have been omitted for clarity, and the upper limits to their observed fluxes are indicated with downward pointing triangles. The six detections are indicated by points with error bars in both x and y; the one with $f_{15,\mathrm{predicted}} \ll f_{15,\mathrm{observed}}$ has a significant separation between its optical and mid-IR centroids and may be a misidentification. Three Balmer-break galaxies in this field are too red in the far-UV to satisfy the active star formation criterion discussed in § 3.3; their locations on this plot are indicated by smaller triangles for the nondetections and by a point without error bars for the detection. See the electronic edition of the Journal for a color version of this figure.

Readers who do not find Figure 8 persuasive may wish to consider the following. The seven galaxies that we predicted to be brightest have the following ranks in observed flux: 5, 6, >6, 3, >6, 1, 4, where undetected objects are assigned the rank " >6 " because we know only that they are fainter than the six detected objects. Over 90% of the Balmer-break galaxies in the 15 μm image have the observed rank " >6 "; if our UV-predicted 15 μm fluxes were unrelated to the observed fluxes, we would have expected $\sim$90% of the seven objects predicted to be brightest to have the rank " >6 ", but that is not the case. This type of reasoning can be quantified with a version of Kendall's τ generalized for censored data sets by Oakes (1982): of 500 simulated data sets we have made by scrambling the observed rank assigned to each predicted rank, only two had a generalized τ as large or larger than the real data set. The predicted and observed fluxes of these galaxies evidently display a significant positive correlation; and moreover the fact that the handful of detections have observed fluxes broadly in line with their predicted fluxes suggests that this correlation is consistent with the expected linear correlation $\langle f_{\rm predicted}\rangle = \langle f_{\rm observed}\rangle$.

3.3.2. *Radio*

Eighty-nine of the Balmer-break galaxies from the spectroscopic sample of Adelberger et al. (2000, in preparation) lie within the deep 1.4 GHz image of the Hubble Deep Field recently published by Richards (2000). We estimated rough 1.4 GHz fluxes for this sample by summing the flux within a 2″0 radius aperture surrounding the optical centroid of each object. The measured fluxes are shown in Figure 9. For the 1 σ uncertainty we took $\sim$12 μJy, the observed rms when we estimated fluxes in a similar manner for random locations in Richards's (2000) image. The predicted fluxes were estimated using

$$f_{\nu,\rm obs}(20\ {\rm cm}) \sim 10^{-0.4(U_n-24.19)}\left[\frac{\mathscr{K}_U(z,\beta)}{1}\right] \times \left(\frac{\mathscr{K}_L}{6.9\times10^5}\right)^{-1}(10^{0.4(4.43+1.99\beta)}-1)\ \mu{\rm Jy}\ , \qquad (18)$$

which follows from equations (4), (5), (7c), and (17). Otherwise the predicted radio fluxes were derived in an identical manner to the predicted mid-IR fluxes in § 3.3.1. The uncertainty in the predicted fluxes arises from the scatter in the β/far-IR correlation (0.3 dex), from the scatter in the far-IR/radio correlation (0.2 dex), from photometric uncertainties in U_n magnitudes (0.1 dex), and from the uncertainty in β due to photometric errors in $U_n - G$ (0.4 dex). Added in quadrature these amount to a $\sim$0.5 dex uncertainty in the predicted 20 cm flux for each object.

Because of the large uncertainties in the predicted and observed fluxes, these data can hardly provide a rigorous test of whether $z \sim 1$ galaxies obey the correlations between far-UV, far-IR, and radio properties observed in rapidly star-forming galaxies in the local universe. However, despite the unimpressive appearance of Figure 9, the data do strongly suggest that the predicted and observed fluxes of Balmer-break galaxies are at least positively correlated: fewer than 1% of simulated data sets generated by randomly shuffling the observed and predicted fluxes had a Kendall's τ as large as the observed data set. The trend of higher measured fluxes for objects with higher predicted fluxes is illustrated by the dotted crosses in Figure 9, which show the mean measured flux ($\pm$ the standard deviation of the mean) for objects in different bins of predicted flux. Although objects with higher predicted fluxes clearly tend to have higher observed fluxes, it appears that the measured 20 cm fluxes may be somewhat lower than our predictions, especially for the brightest objects. The significance of this result is difficult to assess without running Monte Carlo simulations similar to those discussed in § 3.2. These simulations are not yet available.

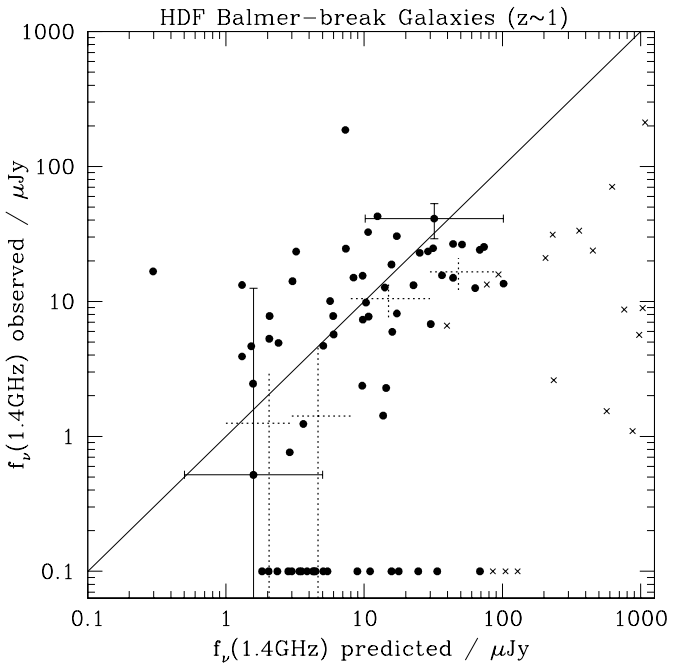

FIG. 9.—Predicted and observed 20 cm fluxes of Balmer-break galaxies at $z \sim 1$. For clarity uncertainties are shown for only a few representative points. Galaxies with observed fluxes lower than 0.1 μJy are shown on the plot at 0.1 μJy. The locations of Balmer-break galaxies too red to satisfy the active star formation criterion of § 3.3 are indicated with solid crosses. The larger dotted crosses indicate the mean observed flux and standard deviation of the mean for galaxies in different bins of predicted flux. One outlier was excluded from the calculation of the mean and standard deviation in its bin of predicted flux, the galaxy with $f_{\rm pred} \simeq 7.5$, $f_{\rm obs} \simeq 200$, which likely has a significant AGN contribution to its measured flux. See the electronic edition of the Journal for a color version of this figure.

3.4. *HR 10*

The $z = 1.44$ galaxy HR 10 initially attracted the attention of Hu & Ridgway (1994) because of its unusually red optical-to-infrared color. Those authors suggested that HR 10 was a high-redshift elliptical galaxy, but subsequent observations provided hints that HR 10 was actively forming stars and suggested that its red colors might result from extreme dust reddening rather than from an aged stellar population (Graham & Dey 1996) This interpretation has received strong support from the recent detection of HR 10 at 450 and 850 μm. HR 10 is now considered the prototypical example of an extremely dusty star-forming galaxy at high redshift. Its photometry is presented in Figure 10 (Dey et al. 1999; Haynes et al. 2000).

Because of the large uncertainties in its rest-frame far-UV colors, we cannot reliably measure β for HR 10, but we can use its observed ratio of far-UV to far-IR luminosity to estimate the value of β required for this object to satisfy MHC's β/far-IR relation. This slope, shown in Figure 10, is not obviously inconsistent with the data.

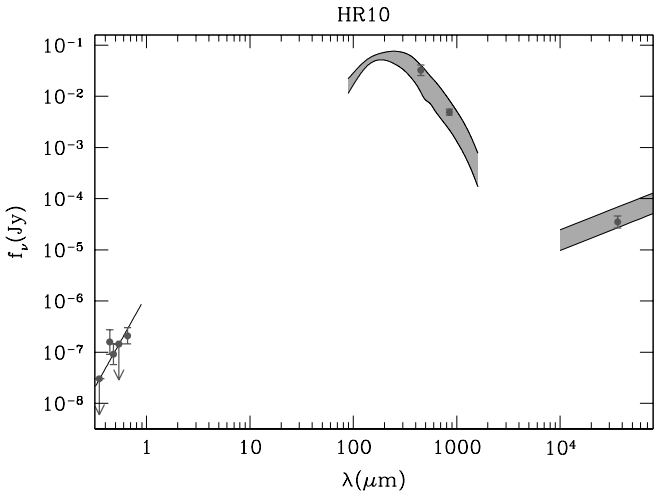

FIG. 10.—Far-UV to radio SED of HR 10. The shaded regions, adjusted vertically to match the observed 450 μm, 850 μm, and 3.6 cm photometry, show ± 1 σ uncertainties on the shape of this galaxy's far-IR and radio emission under the assumption that it obeys the local FIR/radio correlation and has a dust SED similar to those of actively star-forming galaxies in the local universe. The very uncertain (rest) far-UV photometry for this galaxy does not allow us to estimate its far-UV spectral slope β; the solid line in the UV indicates the slope that MHC's β/far-IR relation would predict. HR 10 has a far higher ratio of far-IR to far-UV luminosity than the other galaxies we have considered, and it would not be included in most UV-selected surveys despite its large star formation rate. See the electronic edition of the Journal for a color version of this figure.

Although it is unclear if HR 10 satisfies the β/far-IR relation, we can say with confidence that its ratio of far-IR to UV luminosity far exceeds that of any other galaxy discussed in this section. Despite the large star formation rate implied by its 850 μm flux, HR 10 would not be included in most optically selected high-redshift surveys. Placed at $z = 3.0$, for example, HR 10 would be too faint and too red to satisfy commonly used "Lyman-break" photometric selection criteria (e.g., Steidel, Pettini, & Hamilton 1995). If most of the star formation in the universe occurred in objects like HR 10, rather than in the relatively UV-bright Balmer-break and Lyman-break galaxies previously discussed, then UV-selected high-redshift surveys will provide a seriously incomplete view of star formation in the universe. But this seems an unlikely possibility to us, as we will now explain.

4. UV-SELECTED POPULATIONS, SUB-MILLIMETER SOURCES, AND THE FAR-INFRARED BACKGROUND

In § 3 we tried to assess whether the star formation rates of known high-redshift galaxies can be estimated from their fluxes through various atmospheric windows. Our conclusions were uncertain but hopeful: the meager available evidence is at least consistent with the idea that ground-based observations can be used together with locally calibrated correlations to provide rough constraints on high-redshift galaxies' star formation rates. But estimating moderately accurate star formation rates is only one step toward the ultimate goal of high-redshift surveys, producing a reasonably complete census of star formation at high redshift that can be used to constrain our empirical and theoretical understanding of the early stages of galaxy formation. In this section we will set aside the object-by-object comparisons of star formation rates estimated from photometry at different wavelengths, and turn our attention instead to the larger question of whether existing surveys are approaching the reasonably complete view of high-redshift star formation that we desire.

There is good reason to be concerned that the view of high-redshift star formation provided by these surveys is far from complete. Few star-forming galaxies in the local universe would be included in existing surveys if they were placed at high redshift. This is illustrated by Figure 11*a*, which shows the ratio of dust to ultraviolet luminosity for local galaxies with various star formation rates. For this plot we have adopted $L_{1600} + L_{\rm bol,dust}$ as a crude measure of star formation rate, though in some cases 1600 Å luminosities and dust luminosities can be powered by processes other than star formation. Because of the different constants of proportionality in the conversions of L_{1600} and $L_{\rm bol,dust}$ to star formation rates, the quantity $1.66L_{1600} + L_{\rm bol,dust}$ (cf. eq. [4]; see also MHC) would likely provide a better measure of star formation rate, but in almost all cases L_{1600} is small compared to $L_{\rm bol,dust}$ and our adoption of the simpler $L_{1600} + L_{\rm bol,dust}$ will not appreciably affect the subsequent discussion.

Solid circles on Figure 11*a* denote UV-selected starbursts from the sample of MHC, discussed earlier in the text; § symbols denote nearby spirals,[4] selected randomly from among the objects present in both the Carnegie Atlas of Sandage & Bedke (1994) and the far-UV catalog of Rifatto, Lango, & Capaccioli (1995); open squares denote three LIRGs (NGC 4793, NGC 5256, and NGC 6090) from the catalog of Sanders, Scoville, & Soifer (1991) which had UV fluxes estimated by Kinney et al. (1993) or Rifatto et al. (1995); and open stars denote the ULIRGs VII Zw 031, IRAS F12112+0305, and IRAS F22691−1808 observed in the far-UV by Trentham, Kormendy, & Sanders (1999). Bolometric dust luminosities were estimated from these galaxies' 60 and 100 μm *IRAS* fluxes as discussed in § 2.4. The adopted conversion from *IRAS* fluxes to bolometric dust luminosities is more appropriate for the starbursts, LIRGs, and ULIRGs in Figure 11*a* than for the spirals, but the resulting errors in the spirals' estimated dust luminosities will not affect our conclusions significantly.

Taken together the galaxies in this plot are representative of those that host the majority of star formation in the local universe: according to Heckman (1998), starbursts and spirals account for roughly equal shares of the bulk of star formation in the local universe, while LIRGs and ULIRGs (galaxies with $L_{\rm FIR} \gtrsim 10^{11}$ $L_\odot$) account for perhaps 6% (Sanders & Mirabel 1996).

The curved lines on this plot show the $z = 3.0$ completeness limits ($\Omega_M = 0.3$, $\Omega_\Lambda = 0.7$) for existing surveys at optical (*solid line*), sub-mm (*dashed line*), and radio (*dotted line*) wavelengths. These lines assume an optical flux limit of $f_\nu[1600 \text{ Å} \times (1 + z)] \gtrsim 0.2$ μJy ($\mathscr{R}_{\rm AB} \lesssim 25.5$), roughly appropriate for the Lyman-break survey of Steidel et al. (1999), a sub-mm flux limit of $f_\nu(850\ \mu\text{m}) \gtrsim 2$ mJy, the confusion limit of SCUBA on the JCMT, and a radio flux limit of $f_\nu(20\text{ cm}) \gtrsim 50$ μJy, the completeness limit of Richards's

[4] NGC 247, NGC 1232, NGC 1313, NGC 1398, NGC 2403, NGC 2683, NGC 2976, NGC 3556, NGC 3623, NGC 3726, NGC 3877, NGC 4178, NGC 4216, NGC 4254, NGC 4303, NGC 4307, NGC 4321, NGC 4522, NGC 4559, NGC 4565, NGC 4592, NGC 4595, NGC 4653, NGC 5055, NGC 5248, NGC 5457, NGC 5806, NGC 5879, NGC 5907, and NGC 6946.

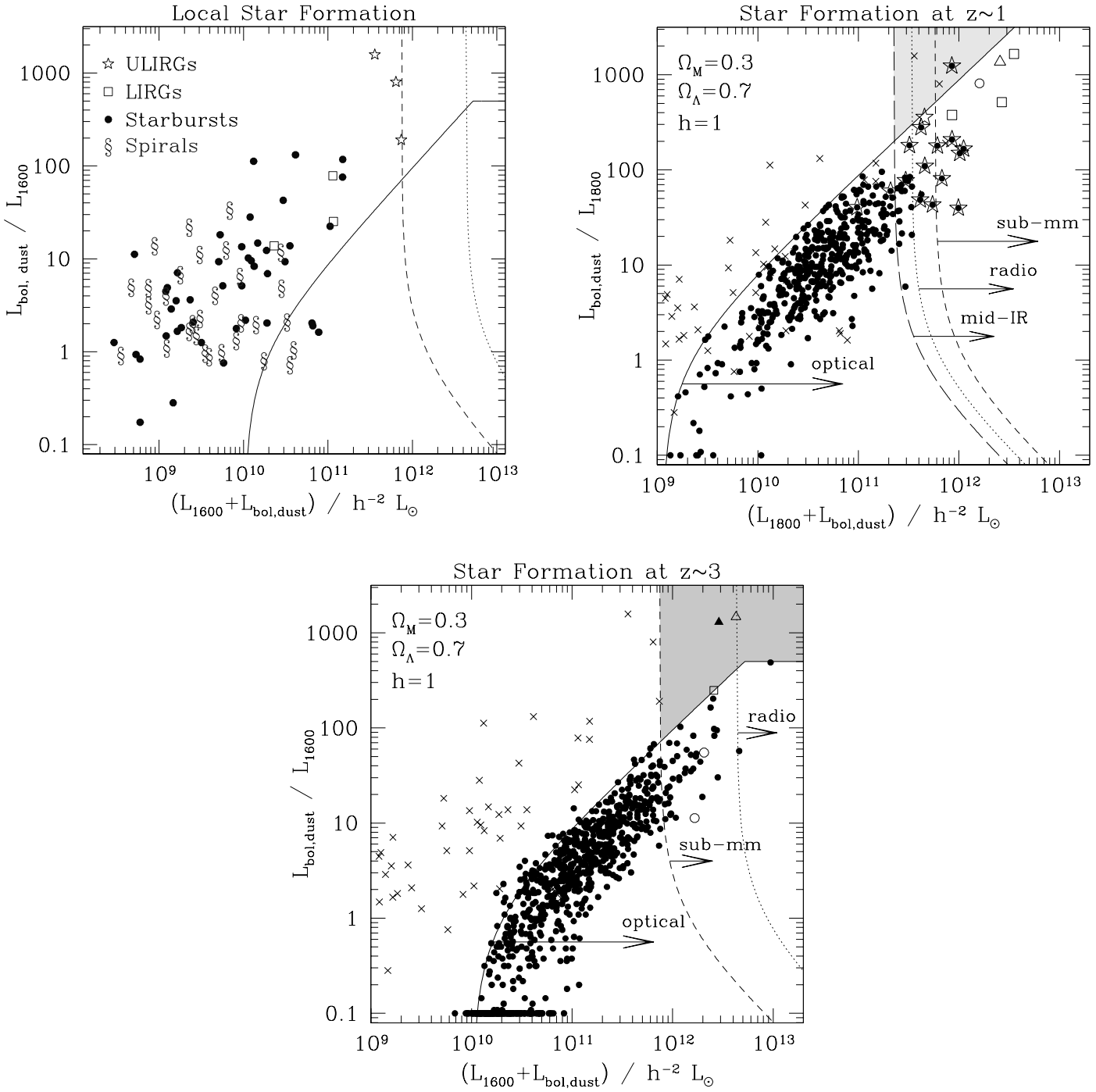

FIG. 11.—(*a*) Star formation in the local universe. The sum $L_{1600} + L_{bol,dust}$, on the abscissa, provides a crude measure of star formation rate; the ratio $L_{bol,dust}/L_{1600}$, on the ordinate, provides a rough measure of dust obscuration. Star formation in the local universe occurs among galaxies with a wide range of luminosities and dust obscuration, and more rapidly star-forming galaxies tend to be more heavily obscured. See text for a description of the four local galaxy samples (spiral, starburst, LIRG, ULIRG) shown. Galaxies similar to those in this plot would not be included in existing optical, sub-mm, or radio surveys at $z \sim 3$, which can detect objects lying to the right of the solid, dashed, and dotted lines. (*b*) Star formation at $z \sim 1$. The abscissa and ordinate are as in (*a*). Solid circles represent optically selected Balmer-break galaxies at $z \sim 1$, stars represent $z \sim 1$ ISO 15 μm sources (15/16 of which are also Balmer-break galaxies), open squares (triangles) represent 850 μm/radio sources with estimated redshifts $z < 2$ from BCR that have detected (undetected) optical counterparts, and the open circle represents HR 10. Crosses mark the positions of the local starbursts, LIRGs, and ULIRGs from (*a*). Galaxies at $z \sim 1$ exhibit a similar correlation of luminosity and dust obscuration as local galaxies. The lines show $z = 1.0$ completeness limits for existing surveys at various wavelengths. Objects in the shaded region of the plot can be detected only through their dust emission. (*c*) Star formation at $z \sim 3$. The abscissa and ordinate are as in (*a*). Solid circles represent optically selected Lyman-break galaxies, open circles represent the optically identified $z \sim 3$ 850 μm sources SMM J14011+0252 and west MMD11, open squares (triangles) represent 850 μm/radio sources with estimated redshifts $z > 2$ from BCR that have detected (undetected) optical counterparts, and the solid triangle represents the optically undetected sub-mm source SMM J00266+1708. Crosses represent local starbursts, LIRGs, and ULIRGs. Solid, dashed, and dotted lines show the approximate $z = 3.0$ completeness limits of existing optical, sub-mm, and radio surveys. Besides a 1600 Å flux limit, the optical line assumes a $G - \mathcal{R}$ color limit of 1.2; the probability that a $z \sim 3$ galaxy will be blue enough to satisfy standard LBG selection criteria declines steadily for $L_{bol,dust}/L_{1600} \gtrsim 20$ and reaches zero by $L_{bol,dust}/L_{1600} \sim 500$—assuming that these galaxies obey MHC's β/far-IR relationship. See Steidel et al. (1999) and Adelberger et al. (2000, in preparation) for a more complete discussion. Any galaxies in the shaded region of this diagram would be detectable in blank-field sub-mm surveys but not in standard optical surveys. See the electronic edition of the Journal for a color version of these figures.

(2000) catalog of HDF sources. Observations with lower flux limits have been obtained in each of these bands, especially the optical—the flux limit in the Hubble Deep Field is nearly an order of magnitude fainter than the 0.2 μJy optical limit we have adopted—but the flux limits above are roughly appropriate for the bulk of existing "deep" observations at each wavelength. Sub-mm and radio flux limits were converted into dust luminosity limits under the assumption that high-redshift galaxies follow the empirical correlations described in § 2. The minimum luminosity for sub-mm detection is roughly independent of redshift, because K-corrections largely cancel out changes in luminosity distance, but the minimum luminosity for optical and radio detection would be (respectively) 7.4 and 13 times fainter at $z \sim 1$ (cf. Figs. 11*b* and 11*c*), and 2.2 and 3.1 times brighter at $z \sim 5$. Evidently, only a small fraction of star-forming galaxies in the local universe would be detected in existing surveys if they were placed at $1 \lesssim z \lesssim 5$.

Nevertheless large numbers of high-redshift galaxies have been found. Figure 11*b* shows the location on the star formation rate versus dust obscuration plot of the majority of known galaxies at $z \sim 1$. Solid circles represent optically selected Balmer-break galaxies at $0.8 < z < 1.2$ from the sample of Adelberger et al. (2000, in preparation), open stars represent 15 μm ISO sources at $0.8 < z < 1.2$ from the HDF sample discussed in § 4.2 below, open squares (triangles) represent radio and sub-mm sources with estimated redshifts $z < 2$ from the optically detected (undetected) sample of BCR, and the open circle represents HR 10. Each object's dust luminosity was estimated from its available ground-based photometry through the empirical correlations described in § 2. In cases where an object's dust luminosity could have been estimated with more than one of the empirical correlations, we took an estimate from the object's flux in only one wavelength range, with the following order of preference: 850 μm, 15 μm, 20 cm, UV. The dust luminosities of ISO sources in the HDF, for example, were estimated from their 15 μm fluxes (§ 2.2) rather than from their UV spectral slopes (§ 2.3) or radio fluxes (§ 2.4). The curved lines in Figure 11*b* show typical $z = 1.0$ detection thresholds for observations at different wavelengths. The optical, sub-mm, and radio thresholds assume the flux limits discussed above; the mid-IR limit assumes a 15 μm flux limit of 75 μJy, which is roughly appropriate for the HDF catalog of Aussel et al. (1999). Because the objects in this plot do not lie at precisely $z = 1.0$, and because small amounts of data exist with flux limits deeper than the typical values adopted here, some detected objects have star formation luminosities $L_{1800} + L_{\rm bol,dust}$ lower than the indicated thresholds.

Figure 11*c* is a similar plot for galaxies at $z \sim 3$. The solid circles represent optically selected Lyman-break galaxies from the sample of Steidel et al. (2000, in preparation), open circles represent the sub-mm sources SMM J14011+0252 and west MMD11, the open squares (triangles) represent radio/sub-mm sources with estimated redshifts $z > 2$ from the optically detected (undetected) sample of BCR, and the solid triangle is the optically undetected sub-mm source SMM J00266+1708 with an estimated redshift $z \sim 3.5$ (Frayer et al. 2000). In this plot (and in Fig. 17 below) the gravitational lensing magnification of SMM J14011+0252 and SMM J00266+1708 was roughly corrected by dividing their observed luminosities by 2.75 (Frayer et al. 1999) and 2.4 (Frayer et al. 2000), respectively.

At each of these redshifts, $z \sim 0$, $z \sim 1$, and $z \sim 3$, star-forming galaxies appear to have a similar range of dust obscuration $0.1 \lesssim L_{\rm bol,dust}/L_{\rm UV} \lesssim 1000$, and to follow a similar correlation of dust obscuration and star formation rate, but the bolometric star formation luminosities of detected galaxies increase steadily from $z \sim 0$ to $z \sim 1$ to $z \sim 3$. This is partly a selection effect, but it also reflects a genuine increase in the number density of rapidly star-forming galaxies at higher redshifts (e.g., Lilly et al. 1996; Steidel et al. 1999; BCR). Although existing high-redshift surveys are not deep enough (for the most part) to detect star-forming galaxies similar to those in the local universe, the observed increase in bolometric star formation luminosity with redshift suggests that these surveys may nevertheless have detected a substantial fraction of high-redshift star formation.

The goal of this section is to estimate how large a fraction of high-redshift star formation they have detected. Have these surveys detected the majority of high-redshift star formation, or only the relatively small fraction that comparison to the local universe might make us expect? Although we will be primarily concerned with the possibility that dust obscuration has hidden large amounts of star formation from existing surveys, other physical effects—surface brightness dimming (e.g., Lanzetta et al. 1999) is an obvious example—can make high-redshift star formation undetectable as well. The results in this section will provide a rough limit on the amount of high-redshift star formation that is undetected in existing surveys.

This limit can be estimated because the brightness of the 850 μm background provides an upper limit on the total amount of star formation at high redshift. Since K-corrections at 850 μm largely cancel out changes in luminosity distance, a galaxy with given bolometric dust luminosity will appear almost equally bright at 850 μm for any redshift in the range $1 \lesssim z \lesssim 5$ (e.g., Blain & Longair 1993). Taken together with the observation that star-forming galaxies emit the majority of their luminosities in the far-IR (cf. Figs. 11*a*–11*c*), this implies that a flux-limited 850 μm survey is nearly equivalent to a star formation–limited survey at $1 \lesssim z \lesssim 5$ and that the integrated 850 μm background provides upper limit to the total amount of star formation at high redshift. It is an upper limit, rather than a measurement, because some fraction of the 850 μm background is known to be produced by objects other than star-forming high-redshift galaxies (e.g., AGN and low-redshift galaxies: Edge et al. 1999; Ivison et al. 2000).

Our strategy for placing limits on the amount of undetected star formation at high redshift will be to calculate the contribution to the 850 μm background from the various known high-redshift populations represented in Figures 11*b* and 11*c* and to see if there is significant shortfall between the background contribution from these galaxies and the total background that is observed.

4.1. *Sub-mm Sources*

We begin by reviewing the contribution to the 850 μm background from resolved sub-mm sources. According to Barger, Cowie, & Sanders (1999a), 20%–30% of the 850 μm background is produced by objects brighter than SCUBA's 2 mJy confusion limit. Understanding the nature of these objects is difficult, because the large diffraction disk of SCUBA on the JCMT means that most have several plausible optical counterparts, but multiwavelength obser-

vational programs (e.g., Frayer et al. 1999; Dey et al. 1999; BCR; Chapman et al. 2000; Frayer et al. 2000, Ivison et al. 2000) have established robust optical counterparts for a handful of them. This work has shown that approximately half of the detected 850 μm sources are associated with AGN (Ivison et al. 2000). Of the sources which do not appear to be AGN, three—SMM J14011+0252 (Frayer et al. 1999), HR 10 (Dey et al. 1999), and west MMD11 (Chapman et al. 2000)—are robustly associated with high-redshift star-forming galaxies. These galaxies, shown in Figures 11*b* and 11*c*, have relatively large dust obscurations $30 < L_{\rm bol,\,dust}/L_{\rm UV} < 1000$ and large implied star formation rates, but their UV luminosities are comparable to those of typical optically selected galaxies at similar redshifts. BCR have shown that the brightest 850 μm sources tend to be even more heavily obscured: their analysis suggests that $\sim$75% (6/8) of 850 μm sources brighter than 6 mJy have extreme dust obscurations $300 < L_{\rm bol,\,dust}/L_{\rm UV} < 3000$, (cf. Figs. 11*b* and 11*c*). The ratio of dust to UV luminosity for these sources is very uncertain because their redshifts (and consequently luminosity distances) are unknown, but BCR's radio/sub-mm photometric redshifts (cf. § 2.4) would have to be seriously in error to bring their estimated dust obscurations into a less extreme range. Despite the large star formation rates implied by their sub-mm fluxes, objects similar to those in the sample of BCR account for only a tiny fraction, $\sim$5% (Barger et al. 1999a), of the measured 850 μm background (Fixsen et al. 1998).

The large dust obscurations observed in 850 μm sources have excited the interest of numerous authors (e.g., Smail et al. 1998; Hughes et al. 1998; Eales et al. 1999; Barger et al. 1999a; Sanders 1999; BCR), who have rightly noted that if fainter high-redshift galaxies had similar levels of dust obscuration, the majority of high-redshift star formation would have occurred in objects that could not be detected in any existing survey (cf. Figs. 11*b* and 11*c*). This popular argument for "hidden" star formation at high redshift is based on analysis of galaxies responsible for only a small fraction of the 850 μm background, however, and it ignores the strong correlation of dust obscuration and luminosity that is observed at low and high redshift alike (cf. Fig. 11). Compelling arguments for or against the existence of hidden high-redshift star formation will require observations of galaxies with typical star formation rates, not merely those with the extreme star formation rates characteristic of the objects discussed in this subsection. Although some progress can be made at 850 μm through observations of lensed sources (e.g., Smail et al. 1998; Ivison et al. 2000), the best constraints currently come from observations at other wavelengths.

4.2. *Mid-IR Sources*

At $z \sim 1$, 15 μm observations can provide a deeper view of dusty star formation than the sub-mm observations we have just discussed (cf. Fig. 11*b*). The deepest existing large-area 15 μm image, a $\sim$20 arcmin^2 region centered on the Hubble Deep Field, was obtained by the ISO satellite in 1997. In this subsection we will review the properties of the dusty galaxies at $z \sim 1$ detected in the PRETI reduction (Aussel et al. 1999) of these data.

The primary (high-significance) catalog of Aussel et al. (1999) contains 46 15 μm sources. As discussed by Aussel et al. (1999) and Cohen et al. (2000), the majority of these sources ($\gtrsim$80%) can be reasonably associated with relatively bright optical counterparts ($R \lesssim 23$). Although some of the ISO sources may lie close to optically bright galaxies by chance, the fact that so many lie close to optically bright galaxies cannot be a coincidence. Spectroscopic redshifts for 40 of these optical counterparts are provided by Aussel et al. (1999) and Cohen et al. (2000); an additional redshift, $z \simeq 0.94$ for HDF-PM3-22, was obtained by Adelberger et al. (2000, in preparation). 16 of the optical counterparts[5] lie at redshifts $0.8 < z < 1.2$.

These 16 galaxies provide a reasonably complete sample of the $z \sim 1$ galaxies in this part of the sky that have the largest dust luminosities. The limiting dust luminosity for this sample is roughly a factor of 3 lower than the limit of blank-field SCUBA surveys. The sample is not exactly dust-luminosity limited, because of the scatter in the $L_{\rm MIR}/L_{\rm bol,\,dust}$ relationship (§ 2.2), and it is not 100% complete, because redshifts have not been obtained for some of the 15 μm sources in this field,[6] but it is as close an approximation a complete, dust-luminosity–limited sample at high redshift as currently exists.

The bolometric luminosities and dust obscurations of the galaxies in this sample are indicated in Figure 11*b*. Their typical dust obscurations, $L_{\rm bol,\,dust}/L_{\rm UV} \sim 100$, are lower than those of the brighter sub-mm sources at similar redshifts. This trend of lower dust obscuration in fainter sources is also observed in the local universe (Fig. 11*a*).

For the most part, the $z \sim 1$ ISO sources in the HDF appear to be drawn from among the same population of $z \sim 1$ galaxies that is routinely studied in the optical. Most of the sources are included in the (optical) magnitude-limited HDF survey of Cohen et al. (2000), for example, and 15 of 16 satisfy the Balmer-break photometric selection criteria of Adelberger et al. (2000, in preparation) and are included in that $z \sim 1$ optical survey as well. They are not typical of the galaxies in optical populations, as the nondetection at 15 μm of most optically selected HDF galaxies shows, but Figure 11*b* suggests that the $z \sim 1$ ISO population can be naturally interpreted as the high-luminosity, high-obscuration tail of known $z \sim 1$ optical populations. Optically selected galaxies are thought to possess a wide range of dust obscurations, and the analysis of § 4.3.1 (below) suggests that 10^{+7}_{-4}% have the obscurations $L_{\rm bol,\,dust}/L_{\rm UV} \gtrsim 30$ characteristic of ISO sources in the HDF. For $\Omega_M = 0.3$, $\Omega_\Lambda = 0.7$ the comoving number density of Balmer-break galaxies to $U_n(AB) \sim 25.5$ (roughly the faintest U_n magnitude for HDF ISO sources) is $\sim 3 \times 10^{-2}\ h^3$ Mpc^{-3}, and so optical observations would lead us to expect that $\sim 3.0^{+2.0}_{-1.2} \times 10^{-3}$ galaxies per comoving h^{-3} Mpc^3 would have dust obscurations $L_{\rm bol,\,dust}/L_{\rm UV} \gtrsim 30$ similar to those observed among ISO sources. This is roughly equal to the observed comoving number density of $z \sim 1$ ISO sources in the HDF (16 galaxies with $0.8 < z < 1.2$ in $\sim$20 arcmin^2, or $2.4 \times 10^{-3}\ h^3$ Mpc^{-3} for $\Omega_M = 0.3$, $\Omega_\Lambda = 0.7$), showing that the $z \sim 1$ ISO population can be consistently interpreted as the dustiest part of the optical population.

A worrisome aspect of Figure 11*b* is that 10 of the $z \sim 1$ ISO sources are predicted to have detectable radio fluxes

[5] HDF-PM3-1, HDF-PM3-6, HDF-PM3-8, HDF-PM3-9, HDF-PM3-10, HDF-PM3-11, HDF-PM3-19, HDF-PM3-20, HDF-PM3-21, HDF-PM3-22, HDF-PM3-25, HDF-PM3-31, HDF-PM3-34, HDF-PM3-37, HDF-PM3-39, and HDF-PM3-45.

[6] If the 15 μm sources without redshifts have the same redshift distribution as those with redshifts, then perhaps two additional 15 μm sources in this field lie at the redshifts of interest $0.8 < z < 1.2$.

$f_\nu(20\ \mathrm{cm}) \gtrsim 50\ \mu\mathrm{Jy}$, while only two were detected at this level by Richards (2000). Other $z \sim 1$ ISO sources are detected in Richards's 20 cm image at lower flux levels, but the total observed 20 cm flux for the $z \sim 1$ ISO sources, after excluding HDF-PM3-6 and HDF-PM3-20 which have optical spectra suggesting the presence of an AGN (Cohen et al. 2000), is $\sim 360\ \mu$Jy, roughly a factor of 4 lower than the total predicted from the local correlations described in § 2. The implication is that the bolometric dust luminosities of the ISO sources may be on average a factor of ~ 4 lower than indicated in Figure 11*b*, presumably because the ratio of mid-IR luminosity to total dust luminosity is systematically higher at $z \sim 1$ than in the local universe. This possibility only strengthens the main point we aimed to make in this section, that ISO sources have lower dust luminosities $L_{\mathrm{bol,dust}}$ and lower dust obscurations $L_{\mathrm{bol,dust}}/L_{\mathrm{UV}}$ than the brighter SCUBA sources, and does not significantly affect the mid-IR/far-UV comparison of § 3.3.1 which exploited the ranks of observed 15 μm fluxes rather than their absolute values; but it does suggest that estimates of the 850 μm background contribution of ISO sources will be subject to significant uncertainty.

The 850 μm background contribution of galaxies similar to ISO sources can be crudely estimated as follows. If we adopt a version of the mid-IR/$L_{\mathrm{bol,dust}}$ relationship (§ 2.2) that correctly predicts the radio fluxes of $z \sim 1$ ISO sources in the HDF, and use the sub-mm/$L_{\mathrm{bol,dust}}$ relationship of § 2.1, then the total predicted 850 μm flux from the 16 $z \sim 1$ ISO sources in the HDF is ~ 8 mJy, or 0.4 mJy arcmin^{-2}, roughly 3% of the background measured by Fixsen et al. (1998). This number applies only to galaxies in the redshift range $0.8 < z < 1.2$, where ISO 15 μm observations are particularly sensitive due to the PAH features. Because little is known about the number density evolution of bright and highly obscured galaxies similar to ISO sources, it is difficult to estimate the contribution from galaxies outside this redshift interval, but a similar population of galaxies distributed uniformly between $z = 1$ and $z = 5$ would contribute $\sim 40\%$ ($\Omega_M = 0.3$, $\Omega_\Lambda = 0.7$) of the total 850 μm background.

Because of the substantial overlap between ISO sources and galaxies in optical surveys, much of the 850 μm background contribution attributed above to ISO sources will be included as well in our calculation of the background contribution from optically selected galaxies, which we now describe.

4.3. *Optical Sources*

Relatively few high-redshift galaxies have been detected by their dust emission, and the few that have apparently account for less than half of the 850 μm background. The vast majority of known high-redshift galaxies have been found in optical surveys. Can the large numbers of optically selected galaxies account for the remainder of the 850 μm background?

Figures 11*b* and 11*c* illustrate the relationship between optically selected galaxies and the 850 and 15 μm sources we have just discussed. The solid circles in Figure 11*b* represent $z \sim 1$ galaxies from the spectroscopic Balmer-break sample of Adelberger et al. (2000, in preparation). Except in cases where their dust emission has been directly measured, the handful of Balmer-break galaxies with estimated dust obscurations $L_{\mathrm{bol,dust}}/L_{\mathrm{UV}} > 100$ were omitted from this plot due to the large uncertainties in their dust luminosities (cf. § 3.3). Balmer-break galaxies with $U_n(AB) > 25.5$ were also omitted, because at these faint magnitudes the Balmer-break sample suffers from severe selection effects. The solid circles in Figure 11*c* represent Lyman-break galaxies from the spectroscopic sample of Steidel et al. (2000, in preparation). As described in the introduction to § 4, the dust luminosities of the optically selected galaxies in Figures 11*b* and 11*c* were estimated from their dust emission in the few cases where it was measured, and from their UV photometry in the typical cases where it was not.

These figures support the common view (e.g., Eales et al. 1999; BCR; Frayer et al. 2000) that galaxies detected in the UV are typically far less luminous and less obscured than those detected in the IR. In the next sections we will see if UV-selected populations can make up in number what they lack in luminosity and still produce a significant contribution to the 850 μm background.

4.3.1. *The 850 μm Luminosity Function of Lyman-Break Galaxies*

As a first step we will estimate the contribution to the 850 μm background from the best understood population of UV-selected high-redshift galaxies: the Lyman-break galaxies at $z \sim 3$. Figure 12 shows these galaxies' apparent magnitude and β distributions (Steidel et al. 1999; Adelberger et al. 2000, in preparation). Adelberger et al. (2000, in preparation) find no significant correlation between appar-

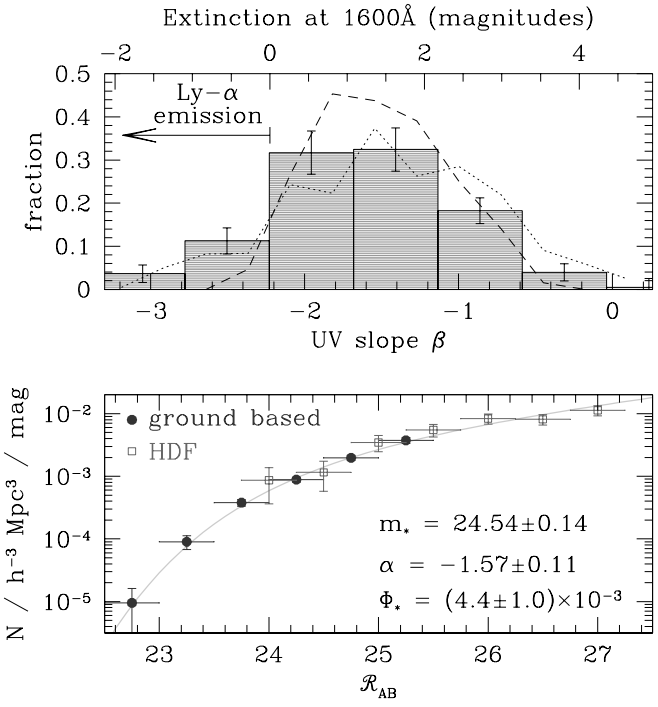

FIG. 12.—Apparent magnitude and β distributions of Lyman-break galaxies at $z \sim 3$, from Steidel et al. (1999) and Adelberger et al. (2000, in preparation). The shaded β distribution is our current best estimate. Systematic uncertainties is the shape of this distribution are probably larger than the random uncertainties denoted by the error bars. This is illustrated by the dotted and dashed lines, which show, respectively, a previous estimate of the β distribution (derived by Steidel et al. 1999 with a crude treatment of photometric errors and incompleteness) and the β distribution derived by correcting for spectroscopically observed Lyα emission but not for our photometric errors and incompleteness. The small differences between these distributions in their red tails have significant consequences; see below. The number density in the luminosity function assumes $\Omega_M = 0.3$ and $\Omega_\Lambda = 0.7$. See the electronic edition of the Journal for a color version of this figure.

ent magnitude and β for Lyman-break galaxies in their ground-based sample ($\mathscr{R} \leq 25.5$; a scatter plot of UV-luminosity vs. dust obscuration in $z \sim 3$ galaxies is presented in Figure 17 and discussed in § 4.4 below) and so it is relatively simple to turn these two distributions into an 850 μm luminosity function. The result is shown in Figure 13. To produce this plot in a way that accounted for the various uncertainties, we first generated a large number of random realizations of Lyman-break galaxies' apparent magnitude and β distributions, consistent to within the errors with the distributions of Figure 12. We then picked at random a β distribution and an apparent magnitude distribution from among these realizations, generated a long list of $\mathscr{R}$, β pairs, with $\mathscr{R}$ drawn randomly from the best Schechter-function fit to the apparent magnitude distribution and β from the β distribution, assigned to each $\mathscr{R}$, β pair in the list an 850 μm flux with equation (8), and adjusted each of these 850 μm fluxes at random by an amount reflecting the uncertainty in their predicted values (see § 3). Binning this list and dividing by the appropriate volume produced one realization of the 850 μm luminosity function shown in Figure 13. We repeated the process, choosing a different realization of the β and apparent magnitude distributions each time, until we had many binned realizations of the expected 850 μm luminosity function. The points shown in Figure 13 are the mean values among these many binned realizations; the uncertainties are the standard deviations. Also shown in Figure 13 are two related luminosity functions estimated in a similar manner: the expected 60 μm luminosity function of Lyman-break galaxies (similar in shape to their bolometric

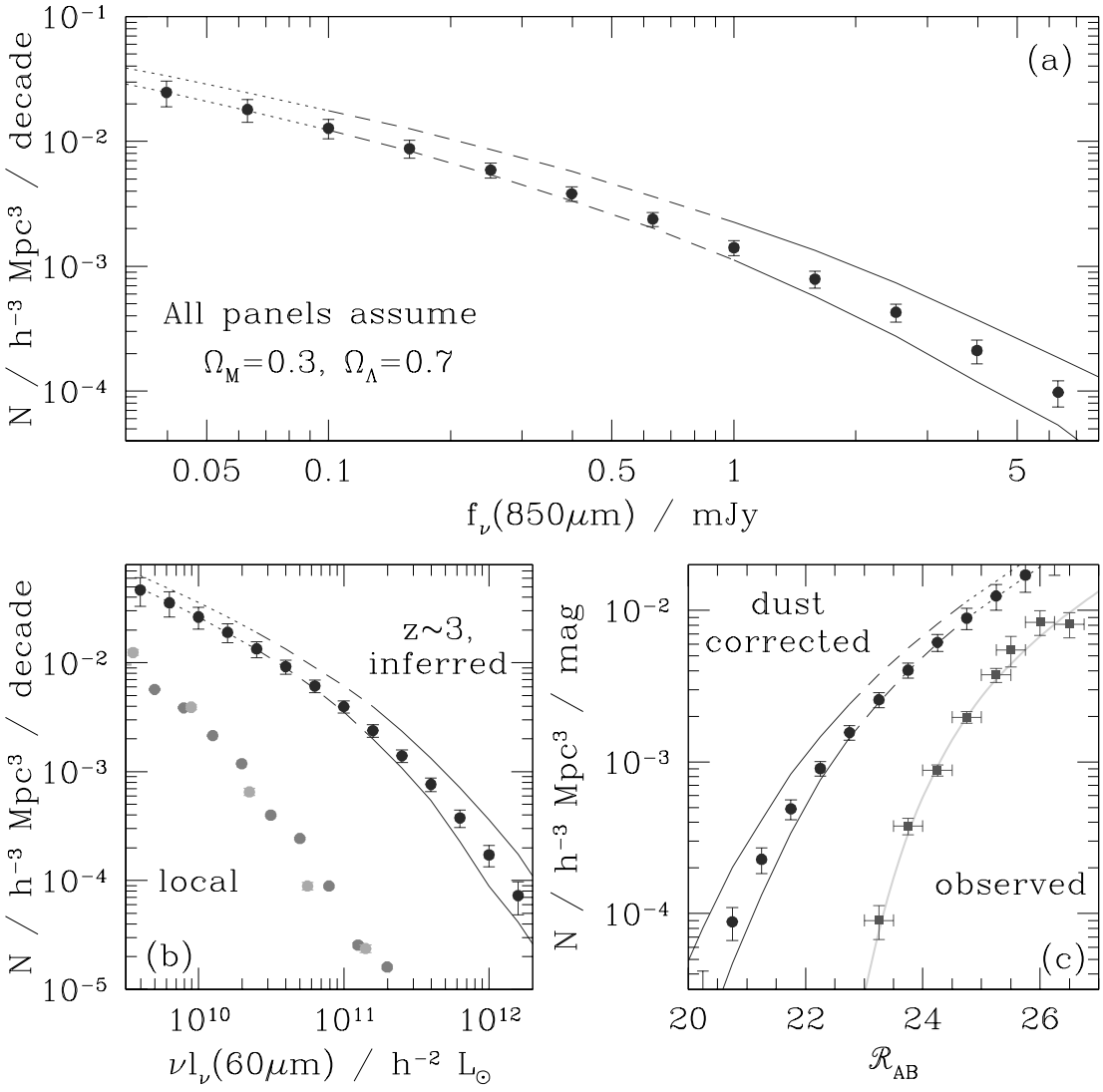

FIG. 13.—(*a*) 850 μm flux distribution of Lyman-break galaxies as inferred from their UV properties. The points in the flux distribution our best estimate; their error bars include the random uncertainties discussed in the text. The curved envelope surrounding these points shows the much larger uncertainty in the 850 μm flux distribution due to possible systematic errors in our derived β distribution. At the faintest fluxes (*dotted envelope*) the expected contribution from sources with $\mathscr{R} > 27$ accounts for most of the estimated 850 μm flux distribution. At slightly higher fluxes (*dashed envelope*) the contribution from sources with $\mathscr{R} > 25.5$ dominates. The inferred flux distribution is most secure at the brightest fluxes (*solid envelope*) that are dominated by the contribution from galaxies with $\mathscr{R} < 25.5$. (*b*) Comparison of the local 60 μm luminosity function (Lawrence et al. 1986; Soifer et al. 1987) to the inferred 60 μm luminosity function of Lyman-break galaxies at $z \sim 3$. Symbols are as in (*a*). (*c*) The observed and dust corrected far-UV luminosity functions of Lyman-break galaxies at $z \sim 3$. The observed luminosity function is from Steidel et al. (1999); the dust corrected luminosity function was estimated as described in the text. Symbols are as in (*a*). See the electronic edition of the Journal for a color version of this figure.

dust luminosity function) and the "dust corrected" UV luminosity function (derived by taking $A_{1600} = 4.43 + 1.99\beta$ for the extinction in magnitudes at 1600 Å, as suggested by MHC). The shapes of these two luminosity distributions, both essentially equivalent to the star formation rate distribution, are similar to what is predicted by the simplest hierarchical models of galaxy formation (Adelberger 2000; Adelberger et al. 2000, in preparation).

The systematic uncertainties in these luminosity functions are far larger than the random uncertainties. The most obvious systematic uncertainty is in the validity of our underlying assumption that the β/far-IR correlation will hold at high redshift. This uncertainty is difficult to treat quantitatively. If the β/far-IR correlation does not hold these results are meaningless; the data in § 3 give us hope that it may hold; there is little else to say.

A second source of systematic uncertainty is the unknown shape of the apparent magnitude distribution at magnitudes fainter than $\mathscr{R} \sim 27$. Galaxies so faint in the UV may still have large star formation rates if they are sufficiently dusty, and so our estimate of the number density of high star formation rate galaxies depends to some degree on the unknown number density of these faint galaxies. In our calculation above we assumed that the $\alpha \sim -1.6$ faint-end slope of the apparent magnitude distribution would continue to arbitrarily faint magnitudes. This extrapolation has a significant effect on our conclusions only at the faintest luminosities; Figure 13 shows the luminosities below which most of the estimated luminosity density comes from objects with $\mathscr{R} > 27$. These parts of the luminosity functions should be viewed with considerable scepticism.

A related source of systematic uncertainty is our assumption that the β distribution of Lyman-break galaxies is the same at all apparent magnitudes. This is known to be true only for $\mathscr{R} < 25.5$ (Adelberger et al. 2000, in preparation), and so the faintest points in our inferred luminosity functions are subject to further systematic uncertainties which are difficult to quantify. This source of systematic uncertainty is negligible only at the brightest luminosities, where most of the estimated luminosity density comes from galaxies with $\mathscr{R} < 25.5$; see Figure 13.

The final source of significant systematic uncertainty is the shape of the β distribution. Deriving this distribution from our data is difficult. It requires (among other things) a quantitative understanding of the selection biases that result from our photometric selection criteria and of the effects of photometric errors and Lyα emission/absorption on our measured broadband colors. Our current best estimate of the β distribution is shown in Figure 12 (Adelberger et al. 2000). To give some idea of the systematic uncertainty in this distribution, we also show our previously published estimate (adapted from Steidel et al. 1999) and the β distribution we would derive if we neglected photometric errors and incompleteness corrections altogether and simply corrected the measured broadband colors for the spectroscopically observed Lyα equivalent width. The most important difference between these three distributions (for our present purposes) is the shape of their red tails. The true shape almost certainly falls within the range they span; it is unlikely to be redder than the distribution of Steidel et al. (1999), and, since all known selection biases cause the Lyman-break technique to miss the reddest objects at $z \sim 3$, it cannot be bluer than the distribution that neglects completeness corrections. The luminosity functions that we would infer given these two limiting β distributions are shown in Figure 13 by curved lines. The systematic uncertainty in the β distribution means that the mean extinction at 1600 Å for Lyman-break galaxies, a factor of 6 in our best estimate, could lie between a factor of 5 and a factor of 9.

4.3.2. *UV-Selected Populations and the* 850 μm *Background*

In this section we will extend the preceding calculation to derive a crude estimate of the total contribution to the 850 μm background from known UV-selected populations at $1 < z < 5$. § 4.3.1 described the uncertainties affecting our calculation of $z \sim 3$ Lyman-break galaxies' contribution to the 850 μm background. Because relatively little is known about UV-selected populations at redshifts other than $z \sim 3$, the uncertainties in the present calculation will be much larger still. As a first approximation we can assume that these galaxies will have the same $\sim$1800 Å luminosity distribution, the same β distribution, and the same lack of correlation between β and $\sim$1800 Å luminosity as Lyman-break galaxies at $z \sim 3$. This is clearly an oversimplification, but the available data suggest that it might not be seriously incorrect. For example, Lyman-break galaxies at $z \sim 4$ appear to have approximately the same luminosity distribution and (possibly) β distribution as Lyman-break galaxies at $z \sim 3$ (Steidel et al. 1999); Balmer-break galaxies at $z \sim 1$ have far-UV spectral slopes β that lie mainly in the range $-2.2 < \beta < -0.5$ observed in Lyman-break galaxies at $z \sim 3$ (Adelberger et al. 2000, in preparation); and, like Lyman-break galaxies at $z \sim 3$, Balmer-break galaxies at $z \sim 1$ exhibit no significant correlation of β with apparent magnitude at rest-frame $\sim$1800 Å (Adelberger et al. 2000; cf. Fig. 17, which we discuss below). The available data suggest further that the comoving star formation density in UV-selected populations is roughly constant for $1 < z < 5$ (Steidel et al. 1999), and so the contribution to the 850 μm background from UV-selected high-redshift populations can probably be crudely approximated as the contribution that would arise from Lyman-break–like populations distributed with a constant comoving number density at $1 < z < 5$.

To estimate this contribution we simulated an ensemble of $\sim 10^6$ Lyman-break–like galaxies at $1 < z < 5$. Each galaxy was assigned a UV slope β drawn randomly from the (*shaded*) β distribution shown in Figure 12; a redshift z_i drawn randomly from the interval $1 < z < 5$ with probability proportional to dV/dz (where dV/dz is the comoving volume per arcmin^2 per unit redshift in an $\Omega_M = 0.3, \Omega_\Lambda = 0.7$ cosmology); an apparent magnitude at rest frame 1600 Å, m_{1600}, drawn randomly from the apparent magnitude distribution in Figure 12 shifted by the ($\Omega_M = 0.3, \Omega_\Lambda = 0.7$) distance modulus between z_i and $z = 3.0$ and truncated at $m_{1600} = 27$; and an observed-frame 850 μm flux with a version of quation (8) appropriate to redshift z_i. Finally, each 850 μm flux was adjusted at random by an amount reflecting the uncertainty in its predicted value (§ 3).

Figure 14 was produced by placing these simulated galaxies into bins of 850 μm flux and dividing by the appropriate area. The top panel shows the estimated contribution to the 850 μm background per logarithmic interval in f_ν, $f_\nu^2 n(f_\nu)$, where $n(f_\nu)$ is the number of sources per mJy per square degree. The overall background expected from UV-selected populations in this crude calculation, 4.1×10^4 mJy deg^{-2}, is close to the measured background of 4.4×10^4 (Fixsen et al. 1998). The closeness of the agree-

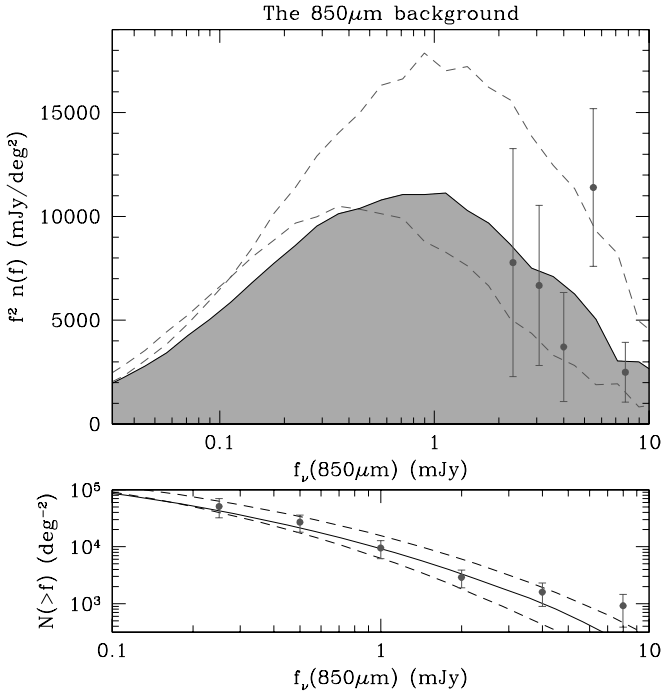

FIG. 14.—*Top panel*: The 850 μm background contribution $f_\nu^2 n(f_\nu)$ from sources with different fluxes. Points with error bars show observed values, derived from data in Barger et al. (1999a); the smooth curves show the background known UV-selected populations at $1 \lesssim z \lesssim 5$ would produce given the simple assumptions described in the text. The solid curve is appropriate to our best estimate of the β distribution. Dashed lines illustrate the uncertainty due to possible systematic errors in our adopted β distribution. This is certainly not the largest source of systematic uncertainty; is it merely the easiest to quantify. The total background for our best-fit β distribution (*shaded region*) is 4.1×10^4 mJy deg^{-2}. The measured 850 μm background is 4.4×10^4 mJy deg^{-2} (Fixsen et al. 1998). *Bottom panel*: The cumulative 850 μm number counts. Symbols are as in the top panel. The observed number counts are from Blain et al. (1999a, 1999b, 1999c). See the electronic edition of the Journal for a color version of this figure.

ment is not especially meaningful, because the uncertainties in the calculation are so large, but nevertheless it is clear that the known UV-selected galaxies at high redshift could easily have produced the $\sim$75% of the 850 μm background that has not currently been resolved into discrete sources by SCUBA. There is little need to invoke large amounts of hidden high-redshift star formation in order to account for the brightness of the 850 μm background.

If the bulk of the 850 μm background is produced by galaxies similar to those in UV-selected surveys, as we have argued, then the shape of the 850 μm number counts should be similar to what our calculation suggests UV selected populations would produce. This appears to be the case. The bottom panel of Figure 14 compares the cumulative 850 μm number counts $N(>f_\nu)$ ($\equiv$the number of objects per square degree brighter than f_ν) measured by Blain et al. (1999b) to the number counts that would be produced by the UV-selected high-redshift galaxies in our calculation. Although there are clear differences at the brightest end, where the observed number counts receive contributions from AGN, from low-redshift galaxies, and from extremely luminous high-redshift galaxies that may differ from the more normal galaxies detected in the UV, the observed number counts are remarkably close to what UV-selected populations would produce in the range 0.3 mJy $< f_\nu <$ 3 mJy that dominates the 850 μm background.

Figure 15 shows the expected contribution to the 850 μm background from objects with different apparent magnitudes at rest-frame 1600 Å. This gives a rough idea of the apparent magnitudes we would expect to measure for sub-mm sources with various fluxes if rest-frame UV-selected populations obeying the local correlations between far-UV and far-IR fluxes produced the bulk of the 850 μm background. At any given 850 μm flux density, objects are expected to have a wide range of redshifts and dust obscurations, and consequently of optical magnitudes, but even at the brightest 850 μm fluxes most objects are expected to be relatively faint ($m_{1600} > 24$) in the optical. The observed faintness of optical counterparts to 850 μm sources is sometimes thought to show that the 850 μm background is produced by objects not present in rest-UV-selected surveys, but this argument has to be made carefully: UV-selected high-redshift galaxies are themselves quite faint in the optical, and as a result it is not sufficient to show (for example) that most optical counterparts are fainter than 24th magnitude; it must be shown instead that they are significantly fainter than Figure 15 predicts. The available data suggest that the sources responsible for brightest 850 μm number counts, $f_\nu \gtrsim 6$ mJy, are in fact significantly fainter than the predictions of Figure 15 (e.g., BCR; Frayer et al. 2000), and this is hardly surprising since our calculation shows that UV-selected populations cannot by themselves account for the brightest 850 μm number counts. Objects with larger obscurations $L_{\rm bol,dust}/L_{\rm UV} \sim 1000$ are required and have been found. Measuring the optical magnitudes of $\sim$1 mJy sources would provide a better test of whether UV-selected populations contribute significantly to the far-IR background, but with current technology this is

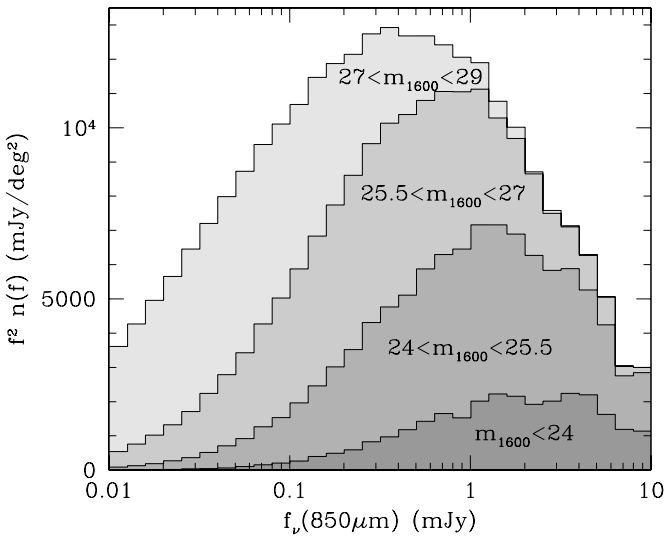

FIG. 15.—Expected contribution to the 850 μm background from UV-selected sources with different apparent magnitudes at 1600 Å rest. Even if UV-selected populations were solely responsible for the 850 μm background, we would expect most of the sub-mm sources brighter than 2 mJy at 850 μm to be fainter than $m_{AB} = 24$ at 1600 Å rest. Also shown is the contribution to the background which would be produced by galaxies with $27 < m_{AB} < 29$ if the $\alpha = -1.6$ faint end slope of the assumed luminosity function continued past the faintest observed magnitude of $m_{1600} \simeq 27$. These galaxies were excluded from the calculation whose results are shown in Fig. 14; see text. See the electronic edition of the Journal for a color version of this figure.

possible only for lensed sources and adequate data do not yet exist.

Also shown in Figure 15 is the contribution to the 850 μm background that would be produced by galaxies with $27 < m_{1600} < 29$ if the $\alpha = -1.6$ faint-end slope of the luminosity function continued past the faintest observed magnitude of $m_{1600} \simeq 27$ and if dust obscuration and reddening remained uncorrelated at the faintest magnitudes. Due to the steep faint-end slope, objects with $m_{1600} > 27$ might be expected to contribute significantly to the 850 μm background. MHC have presented evidence, however, from Lyman-break galaxies with $25.5 \lesssim m_{1600} < 27$ in the HDF, that galaxies fainter in the UV tend to have lower dust extinctions. Because apparent magnitude and dust obscuration are not correlated among $z \sim 3$ Lyman-break galaxies with $m_{1600} < 25.5$, we assumed when producing Figures 14 and 15 that they would remain uncorrelated at fainter magnitudes as well. MHC's analysis suggests that this assumption is incorrect: galaxies with $25.5 < m_{1600} < 27$ are probably somewhat less dusty than we have assumed and galaxies with $m_{1600} > 27$ are probably significantly less dusty. When estimating the total background contribution from UV-selected populations (Fig. 14), we assumed as a compromise that galaxies with $25.5 < m_{1600} < 27$ would be as dusty as galaxies with $m_{1600} < 25.5$ and that galaxies with $m_{1600} > 27$ would contain negligible amounts of dust. This is obviously a very crude solution to a complicated problem; the background contribution from objects with $m_{1600} > 25.5$ is a significant source of systematic uncertainty in Figures 14 and 15.

Figure 15 would be more useful for observational tests if we showed the predicted magnitudes at fixed observed-frame wavelengths, say the i band, rather than a fixed rest-frame wavelength, but this requires us to estimate K-corrections for these galaxies and we have not found an adequate model for their UV/optical SEDs. The problem is illustrated by Figure 16, which shows the measured rest-frame UV/optical SEDs of two Lyman-break galaxies detected at 850 μm, SMM J14011+0252 (Smail et al. 1998) and west MMD11 (Chapman et al. 2000). The optical data were obtained as described in § 3.1 and in Steidel et al. (2000, in preparation); the near-IR photometry was obtained with NIRC (Matthews & Soifer 1994) on Keck I with excellent seeing ($\lesssim$0.″5) in 1999 May. Neither SED is fitted well by a model of a continuously star-forming galaxy subjected to varying amounts of dust following a standard extinction law. Moreover, even though SMM J14011+0252 and west MMD11 have essentially indistinguishable SEDs in the UV—both are consistent with the same value of β—their optical SEDs are significantly different. The shapes of galaxies' UV/optical SEDs are strongly dependent on their star formation histories, and perhaps the simplest conclusion to draw from Figure 16 is that the star formation histories of high-redshift galaxies are complicated and diverse. We have found no obvious way to predict their optical photometry from their UV photometry. See Shapley et al. (2000, in preparation) for a more complete discussion.

This is a good place to remind readers that our UV-based estimates of high-redshift galaxies' bolometric dust luminosities are not derived from an assumed intrinsic SED and dust reddening law; they are derived instead from the empirical (and somewhat mysterious) correlation between β and $L_{\rm bol,dust}/L_{1600}$ described in § 2.3. The diversity of observed SEDs makes it difficult to understand why this

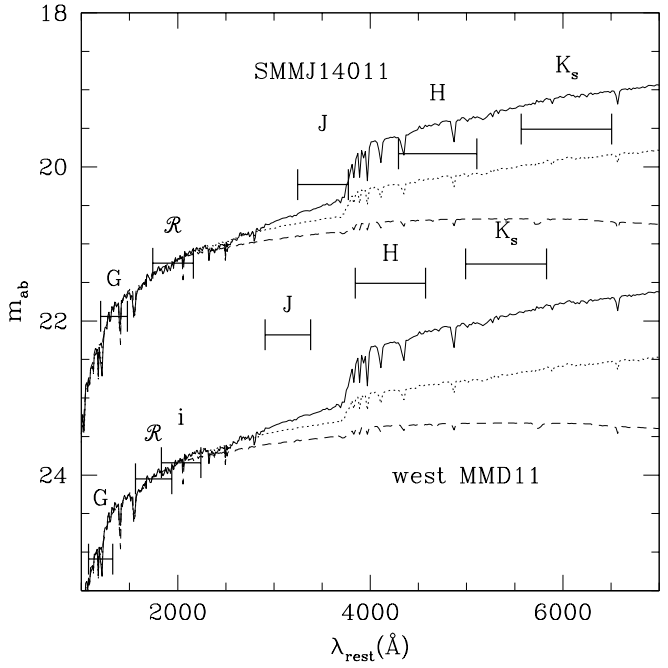

FIG. 16.—UV-to-optical photometry of two $z \sim 3$ galaxies detected at 850 μm. The bars show measured AB magnitudes, and the lines show Bruzual & Charlot (1996) model galaxies after 1 Myr (*dashed line*), 40 Myr (*dotted line*), and 1 Gyr (*solid line*) of star formation at a constant rate. The model SEDs were reddened with dust following Calzetti's (1997) extinction law as required to match the observed $G-\mathcal{R}$ color; for both galaxies this required $A_{1600} = 3.2$ for the 1 Gyr SED, $A_{1600} = 3.9$ for the 40 Myr SED, and $A_{1600} = 4.5$ for the 1 Myr SED. The value of A_{1600} adopted in the text was derived from the empirical correlation between UV spectral slope β and the ratio $L_{\rm bol,dust}/L_{1600}$, not from an assumed SED and dust reddening law. See the electronic edition of the Journal for a color version of this figure.

correlation should exist, but local (§ 2) and (less convincingly) high-redshift (§ 3) observations suggest that it does.

4.4. *Discussion*

The major result of this section is our calculation showing that galaxies similar to those detected in UV-selected surveys probably produced a large fraction of the measured 850 μm background. Recent analyses of 850 μm surveys have reached the opposite conclusion (e.g., Smail et al. 1998; Hughes et al. 1998; Eales et al. 1999; Barger et al. 1999a, Sanders 1999; BCR). Skeptical readers may wonder if our calculation is robust given its apparently heavy reliance on the poorly tested assumption (§ 3) that high-redshift galaxies' dust luminosities can be estimated from their UV fluxes with the correlations of § 2.

Although the details of our calculation certainly depend upon the assumption that high-redshift galaxies obey MHC's β/far-IR relationship, the overall background contribution from UV-selected galaxies depends primarily upon the adopted mean value of $L_{\rm bol,dust}/L_{\rm UV}$. MHC's relationship implies that $\langle L_{\rm bol,dust}/L_{\rm UV}\rangle \simeq 1.66 \times \langle 10^{0.4A_{1600}} - 1\rangle \sim 8$ for galaxies at $z \sim 3$, and our calculation in § 4.3 showed that this factor of 8 is sufficient for UV-selected galaxies to have produced the bulk of the 850 μm background. High-redshift galaxies may not satisfy MHC's relationship, but the adopted $\langle L_{\rm bol,dust}/L_{\rm UV}\rangle \sim 8$ is still a plausible estimate of their mean dust obscuration. This mean obscuration is hardly unrealistically high; it is roughly equal to mean obscuration among the Lyman-

break galaxies observed in the sub-mm by Chapman et al. (2000), for example, and it is lower than the mean obscuration ($\sim$15) in the local UV-selected starburst sample of MHC. Even the local spirals in the sample discussed before § 4.1 have $\langle L_{\rm bol,dust}/L_{\rm UV}\rangle \sim 5$; given the correlation of dust obscuration and star formation rate that appears to exist at all redshifts (cf. Figs. 11*a*–11*c*), it is hard to imagine that a rapidly star-forming population at any redshift could have values of $L_{\rm bol,dust}/L_{\rm UV}$ significantly lower than spirals in the local universe.

But the fundamental difference between our analysis and the analyses of previous authors who reached opposite conclusions is not simply the value of $\langle L_{\rm bol,dust}/L_{\rm UV}\rangle$ adopted for UV-selected galaxies; it is instead the assumed dependence of dust obscuration on luminosity among high-redshift galaxies. Arguments for large amounts of hidden star formation at high redshift generally assume that dust obscuration and luminosity are independent. Data from low and high redshifts lead us to believe that $L_{\rm bol,dust}/L_{\rm UV} \approx L_{\rm bol,dust}$ is a better approximation (cf. Figs. 11*a*–11*c* and 17). This correlation between dust obscuration and luminosity means that the $f_\nu(850\ \mu{\rm m}) \sim 1$ mJy sources that produce most of the 850 μm background are likely to be significantly less obscured than the brighter sources currently detectable in the sub-mm. For example, if the $\sim$10 mJy sources studied by BCR have $200 \lesssim L_{\rm bol,dust}/L_{\rm UV} \lesssim 2000$ (cf. Figs. 11*b* and 11*c*), then the correlation of dust obscuration and luminosity would suggest the 1 mJy sources responsible for most of the 850 μm background have $20 \lesssim L_{\rm bol,dust}/L_{\rm UV} \lesssim 200$. These sources would be dustier than typical optically selected galaxies, but they would nevertheless be as easy to detect in the optical as in the sub-mm. More generally, the correlation of dust obscuration with luminosity means that heavily obscured sources are not necessarily any harder to detect in the rest-frame UV than less obscured sources. Their higher UV obscurations are largely cancelled out by their higher intrinsic luminosities. This is illustrated by Figure 17, which shows the observed UV luminosities of sources with different dust obscurations at low and high redshift. Observed UV luminosities are similar for galaxies with dust obscurations $L_{\rm bol,dust}/L_{\rm UV}$ spanning 4 orders of magnitude.

How robust is the claimed existence of the correlation between dust obscuration and luminosity? At low redshift, where objects' dust luminosities are well constrained by *IRAS* measurements, its existence is indisputable. At higher redshifts, dust luminosities can only be estimated with the uncertain empirical correlations described in § 2, and its existence is somewhat less secure. But even if none of the empirical correlations of § 2 hold at high redshift, it is difficult to escape the conclusion that dust obscuration and luminosity are correlated. Without the correlations of § 2 we would not know precisely where on the x-axis to place any object in Figure 17, for example, but we would still know that ISO sources are typically more luminous and more obscured than optical sources and that SCUBA sources are typically more luminous and more obscured than ISO sources[7]; and that is enough to establish the existence of the correlation.

[7] For example, typical optical sources at $z \sim 1$ are fainter at 15 μm and 20 cm than ISO sources at $z \sim 1$; typical $z \sim 1$ ISO sources must be fainter than typical SCUBA sources, or else they would overproduce the 850 μm number counts.

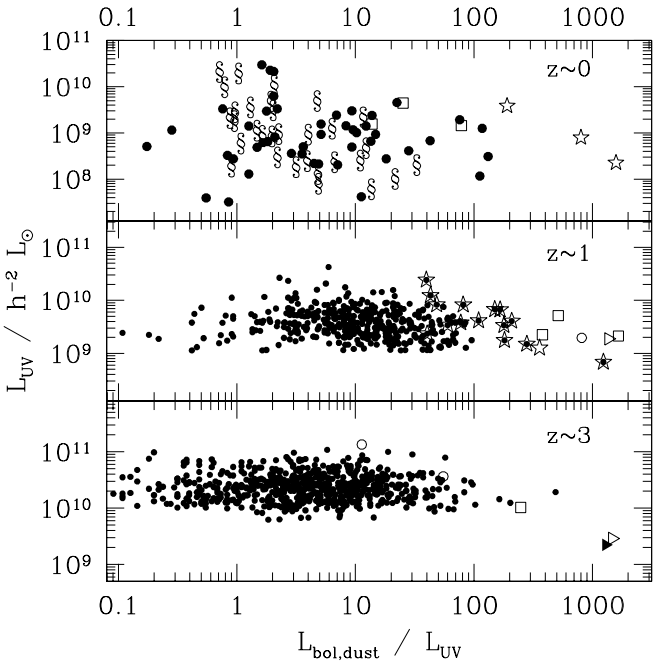

FIG. 17.—Far-UV luminosity vs. dust obscuration for star-forming galaxies at $z \sim 0$ (*top panel*), $z \sim 1$ (*middle panel*), and $z \sim 3$ (*bottom panel*). Symbols are as in Figs. 11*a*–11*c*. Dust absorbs UV photons, but dustier galaxies tend to have higher star formation rates and larger intrinsic UV luminosities, and as a result the observed UV luminosities of star-forming galaxies are largely independent of their dust obscuration. There are exceptions, but in general extremely dusty galaxies are no fainter in the far-UV than relatively dust-free galaxies. The 1600 Å luminosities assume $\Omega_M = 0.3$, $\Omega_\Lambda = 0.7$. Objects represented by open squares, open triangles, and solid triangles do not have spectroscopic redshifts, and their placement on this plot is very uncertain. The lower limits to the UV luminosities of optically selected galaxies at $z \sim 1$ and $z \sim 3$ reflect the flux limits of existing surveys. The apparent increase of UV luminosities with redshift is partly but not solely a selection effect. The color-selection criteria used in constructing the $z \sim 1$ and $z \sim 3$ optical samples result in a selection bias against the bluest objects at $z \sim 1$ and the reddest objects at $z \sim 3$. When selection effects are corrected (as they have been in § 4 but not in this figure) the observed dust obscuration distributions in optical populations at $z \sim 1$ and $z \sim 3$ are similar. See the electronic edition of the Journal for a color version of this figure.

A final and more direct argument that UV-selected galaxies contribute significantly to the 850 μm background comes from the work of Peacock et al. (2000), who showed that positive background fluctuations in a deep 850 μm image of the HDF (Hughes et al. 1998) tend to be coincident with the locations of UV-selected high-redshift galaxies. Their detailed analysis suggests that UV-selected populations must have produced at least one quarter, and probably at least one half, of the total 850 μm background.

Taken together the preceding arguments make a reasonably strong case that the majority of high-redshift star formation is detectable in the deepest optical surveys. But this does not imply that IR/sub-mm observations are unnecessary. Although many of the results that have emerged from sub-mm surveys could have been inferred from UV data alone—the brightness of the 850 μm background, for instance, or the domination of the 850 μm background by $\sim$1 mJy sources (e.g., Blain et al. 1999b; cf. Fig. 14), or the $\sim$thousand-fold increase in number density of ULIRGs from $z \sim 0$ to $z \gtrsim 3$ (e.g., Sanders 1999; cf. Fig. 13)—some could not. For example, there was little indication from UV-selected surveys that extremely dusty galaxies with

$L_{\rm bol,dust}/L_{\rm UV} \gg 100$ even existed (cf. Fig. 12), let alone that they hosted a significant fraction ($\gtrsim 5\%$) of high-redshift star formation. Observations in the IR will continue to play a central role in studies of high-redshift star formation, both as tests of the dust corrections that UV-selected surveys require and as the most efficient way to find the dustiest and most rapidly star-forming galaxies.

5. SUMMARY

The available evidence strongly suggests that dust in high-redshift galaxies will have absorbed most of the UV radiation emitted by their massive stars. Dust certainly absorbs most of the UV radiation emitted by rapidly star-forming galaxies in the local universe, and the ratio of the far-IR to optical backgrounds shows that the situation must have been similar throughout the history of the universe. Estimating the bolometric dust luminosities of high-redshift galaxies is therefore a crucial step in deriving their star formation rates. The first part of this paper was primarily concerned with ways bolometric dust luminosities can be estimated even though most of the dust emission is blocked by the Earth's atmosphere before it can be detected on the ground.

We began in § 2 by describing correlations between local galaxies' bolometric dust luminosities and luminosities at more accessible far-UV, mid-IR, sub-mm, and radio wavelengths. These correlations provide the basis for attempts to estimate high-redshift galaxies' bolometric dust luminosities. Much of this section was simply a review of previously published results; the minor new contribution was a quantification of the uncertainties involved in estimating bolometric dust luminosities from observations at a single rest wavelength $25\ \mu{\rm m} \lesssim \lambda \lesssim 600\ \mu$m or $\lambda \sim 8\ \mu$m. The data suggest that radio, sub-mm, mid-IR, and far-UV estimates of local galaxies' bolometric dust luminosities are all subject to a comparable uncertainty of 0.2–0.3 dex.

Section 3 was concerned with establishing whether the bolometric dust luminosities of high-redshift galaxies can be estimated from their fluxes through various atmospheric windows with the correlations of § 2. The evidence presented was of uneven quality. The galaxy with the highest quality observations, SMM J14011+0252 at $z = 2.565$, obeyed the expected correlations nicely. The observations of more typical $z \sim 3$ galaxies had extremely low signal-to-noise ratios ($\lesssim 1$) and were largely inconclusive, though at least consistent with the expected correlations. Galaxies in our $z \sim 1$ sample were bright enough in the mid-IR and radio for us to show with high significance ($>99\%$) that their predicted and observed fluxes in each of these bands were positively correlated. The data suggested moreover that this positive correlation was at least broadly consistent with the expected linear correlation $\langle f_{\rm observed}\rangle = \langle f_{\rm predicted}\rangle$. Taken together the data in this section make a plausible but still unconvincing case that the bolometric dust luminosities of high-redshift galaxies can be estimated with the expected accuracy using correlations calibrated in the local universe.

Our most important results were presented in the second part of this paper, § 4, where we estimated the contributions to the far-IR background from different high-redshift populations. The brightness of the 850 μm background provides a rough measure of the total amount of star formation at high redshift, and a significant shortfall between the background contribution from known populations and the measured background would show that existing surveys have not detected the majority of star formation at high redshift. We did not find any evidence for a shortfall. The extremely luminous objects currently detectable in the sub-mm can account for $\sim 25\%$ of the far-IR background; the somewhat fainter galaxies detected in the mid-IR by ISO can account for perhaps an additional $\sim 15\%$; and the galaxies detected in optical surveys can account for the remainder. Attributing the far-IR background to different galaxy populations in this way obscures the fact that there is substantial overlap between galaxy populations selected at different wavelengths, especially the mid-IR and optical, but the important point is that the brightness of the 850 μm background is similar to what known high-redshift populations would produce if they obeyed the local correlations of § 2. This casts doubt on recent claims that the majority of high-redshift star formation is hidden from existing surveys (e.g., Lanzetta et al. 1999; BCR).

The analysis of § 4 suggested that the bulk of the 850 μm background was produced by moderately obscured galaxies ($1 < L_{\rm bol,dust}/L_{\rm UV} < 100$) similar to those that host most of the star formation in the local universe and to those that are detected in UV-selected high-redshift surveys. The brightness of the 850 μm background is sometimes cited as evidence that most of the star formation in the universe occurred in dusty objects missing from UV-selected surveys, but this is a mistaken conclusion: the bright 850 μm background shows only that a large fraction of star formation occurred in dusty objects, not that it occurred in the extremely dusty objects ($L_{\rm bol,dust} \gtrsim 100 L_{\rm UV}$) that are easier to detect in the sub-mm than the far-UV. If we assumed that star formation at high redshift occurred only in known UV-selected populations and asked how dusty these galaxies would have to be to produce the observed 850 μm background, we would find that the mean required extinction at 1600 Å was a factor of ~ 6—precisely the value that is generally inferred for UV-selected galaxies at $z \sim 1$ and $z \sim 3$ and similar to the values observed in spirals and UV-selected starbursts at $z \sim 0$. The brightness of the 850 μm background does not by itself require any star formation at all to have occurred in galaxies dustier than the moderately obscured ones ($1 < L_{\rm bol,dust}/L_{\rm UV} < 100$) known to contain most of the star formation in the local universe.

This is not to say that extremely dusty galaxies ($L_{\rm bol,dust}/L_{\rm UV} > 100$) do not exist. Some clearly do (e.g., Dey et al. 1999; BCR; Frayer et al. 2000). Part of the far-IR background is produced by them. Our argument is simply that if high-redshift galaxies are similar to local galaxies in either their typical dust obscurations or their correlation of dust obscuration with luminosity, then UV-selected populations at high redshift must have contributed significantly to the 850 μm background (see § 4.4). The fundamental difference between our analysis and the analyses of previous authors who reached opposite conclusions is the assumption made about the correlation between luminosity and dust obscuration. We have assumed that a correlation exists; they have assumed that it does not. The assumed existence of this correlation strongly affects the amount of high-redshift star formation that is detectable in the optical, since it implies first that the $0.3 < f_\nu(850\ \mu{\rm m}) < 3$ mJy sources which dominate the 850 μm background are likely to be less obscured than the brighter sources detectable with SCUBA, and second that the dustiest, most rapidly star-forming galaxies at high redshift are not necessarily any

harder to detect in the UV than the less obscured sources forming stars at more moderate rates. A correlation similar to the one we have assumed is known to exist in the local universe, and in § 4 we presented evidence that it exists at $z \sim 1$ and $z \sim 3$ as well. As illustrated by Figure 17, the high-redshift galaxies that have been detected by their dust emission are (with few exceptions) no fainter in the UV than the less obscured UV-selected galaxies at comparable redshifts.

Although we have argued that the majority of high-redshift star formation is detected in UV-selected surveys and that many of the recent results from far-IR/sub-mm observations could have been predicted from UV observations alone (e.g., the brightness of the 850 μm background, the shape of the 850 μm number counts, the $\sim$thousand-fold increase in the number density of ULIRGs at high redshift), we do not want to suggest that IR observations are unnecessary. Our arguments imply on the contrary that they are indispensable. Large corrections for dust extinction will be necessary in the interpretation of UV-selected surveys, and only IR observations can show whether the currently adopted corrections are valid or suggest alternatives if they are not. And the fact remains that IR/sub-mm surveys are the most efficient way to find the extremely luminous and dusty galaxies known to produce at least 5% of the 850 μm background.

It is commonly assumed that star formation at high redshift occurs in two distinct populations of galaxies, one relatively unaffected by dust and the other completely obscured. We favor a different view. High-redshift galaxies exhibit a continuum of dust properties. Some contain little dust, and some contain so much dust that they are nearly invisible in the optical; but the majority of star formation occurs in galaxies between these two extremes, in galaxies with $1 < L_{\rm bol,dust}/L_{\rm UV} < 100$. The galaxies in this dominant population are undeniably dusty—most emit a larger fraction of their bolometric luminosities in the far-IR than in the far-UV—but with current technology they are easiest to detect in the rest-frame UV. Because in most cases only a small fraction of their luminosities emerge in the far-UV, large corrections for dust obscuration are required when estimating their star formation rates. A major purpose of this paper was to show that these corrections are tractable and produce sensible results. Although the validity of UV-derived dust corrections has not been convincingly demonstrated on an object-by-object basis, and further observations in the infrared are clearly required, our analysis suggests that the majority of high-redshift star formation occurs in objects which can at least be detected in existing UV-selected surveys. This is good news for those attempting to understand galaxy formation at high redshift, since it is likely that UV-selected surveys will continue to provide the most statistically robust information for at least the next decade.

This paper was made possible by several researchers who generously gave us access to their data during the early stages of its publication. We are grateful to D. Calzetti for her ISO measurements of dust emission from local starbursts, to E. Richards for his 20 cm image of the Hubble Deep Field, and to T. Haynes, G. Cotter, and A. Bunker for the optical magnitudes of HR 10. In addition M. Dickinson, M. Giavalisco, M. Pettini, A. Shapley, and R. Brunner helped obtain some of the data we have presented, and G. Taylor kindly provided us with an estimate of SMM J14011's radio flux prior to its publication by other authors. D. Elbaz recommended looking at the 15 μm fluxes of galaxies in our Balmer-break sample. D. Frayer and A. Barger are thanked for several informative conversations. Useful comments on an earlier draft were provided by A. Blain, M. Dickinson, D. Elbaz, M. Pettini, and (especially) S. Lilly, the referee. C. C. S. acknowledges support from the US National Science Foundation through grant AST 95-96229, and from the David and Lucile Packard Foundation. This research has made use of the NASA/IPAC Extragalactic Database (NED) which is operated by the Jet Propulsion Laboratory, California Institute of Technology, under contract with the National Aeronautics and Space Administration.

REFERENCES

Acosta-Pulido, J. A., et al. 1996, A&A, 315, L121
Adelberger, K. L. 2000, in ASP Conf. Ser. 200, Clustering at High Redshifts, ed. A. Mazure, O. Le Fèvre, & V. Le Brun (San Francisco: ASP), 13
Aussel, H., Cesarsky, C. J., Elbaz, D., & Starck, J. L. 1999, A&A, 342, 313
Barger, A. J., Cowie, L. L., & Richards, E. A. 2000, ApJ, submitted (BCR)
Barger, A. J., Cowie, L. L., & Sanders, D. B. 1999a, ApJ, 518, L5
Barger, A. J., Cowie, L. L., Sanders, D. B., Fulton, E., Taniguchi, Y., Sato, Y., Kawara, K., & Okuda, H. 1998, Nature, 394, 248
Blain, A. W., Jameson, A., Smail, I., Longair, M., Kneib, J.-P., & Ivison, R. 1999a, MNRAS, 309, 715
Blain, A. W., Kneib, J.-P., Ivison, R. J., & Smail, I. 1999b, ApJ, 512, L87
Blain, A. W., & Longair, M. S. 1993, MNRAS, 264, 509
Blain, A. W., Smail, I., Ivison, R. J., & Kneib, J.-P. 1999c, MNRAS, 302, 632
Calzetti, D. 1997, AJ, 113, 162
Calzetti, D., Armus, L., Bohlin, R. C., Kinney, A. L., Koornneeff, J., Storchi-Bergmann, T., & Wyse, R. F. G. 1999, ApJ, 543, 682
Carilli, C. L., & Yun, M. S. 1999, ApJ, 513, L13
———. 2000, ApJ, 530, 618
Chapman, S., et al. 2000, MNRAS, in press
Cohen, J., Hogg, D., Blandford, R., Cowie, L., Hu, E., Songaila, A., Shopbell, P., & Richberg, K. 2000, ApJ, 538, 29
Condon, J. J. 1992, ARA&A, 30, 575
Dey, A., Graham, J. R., Ivison, R. J., Smail, I., Wright, G. S., & Liu, M. C. 1999, ApJ, 519, 610
Dunne, L., Eales, S., Edmunds, M., Ivison, R., Alexander, P., & Clements, D. L. 2000, MNRAS, 315, 115
Eales, S., Lilly, S., Gear, W., Dunne, L., Bond, J. R., Hammer, F., Le Fèvre, O., & Crampton, D. 1999, ApJ, 515, 518
Edge, A. C., Ivison, R. J., Smail, I., Blain, A. W., & Kneib, J.-P. 1999, MNRAS, 306, 599
Fixsen, D. J., Dwek, E., Mather, J. C., Bennett, C. L., & Shafer, R. A. 1998, ApJ, 508, 123
Flores, H., et al. 1999, ApJ, 517, 148
Frayer, D. T., et al. 1999, ApJ, 514, L13
Frayer, D. T., Smail, I., Ivison, R. J., & Scoville, N. Z. 2000, AJ, submitted
Freedman, W., & Madore, B. 1988, ApJ, 332, L63
Graham, J. R., & Dey, A. 1996, ApJ, 471, 720
Haynes, T., et al. 2000, MNRAS, submitted
Heckman, T. 1998, in ASP Conf. Ser. 148, Cosmic Origins of Galaxies, Planets, and Life, ed. J. M. Shull, C. Woodward, & H. Thronson (San Francisco: ASP), 127
Helou, G., Khan, I. R., Malek, L., & Boehmer, L. 1988, ApJS, 68, 151
Holland, W. S., et al. 1999, MNRAS, 303, 659
Hu, E. M., & Ridgway, S. E. 1994, AJ, 107, 1303
Hughes, D. H., Gear, W. K., & Robson, E. I. 1990, MNRAS, 244, 759
Hughes, D. H., et al. 1998, Nature, 394, 241
Ivison, R. J., et al. 2000, MNRAS, 315, 209
Kells, W., Dressler, A., Sivaramakrishnan, A., Carr, D., Koch, E., Epps, H., Hilyard, D., & Pardeilhan, G. 1998, PASP, 110, 1489
Kinney, A. L., Bohlin, R. C., Calzetti, D., Panagia, N., Wyse, R. F. G. 1993, ApJS, 86, 5
Klaas, U., Haas, M., Heinrichsen, I., & Schulz, B. 1997, A&A, 325, L21
Lanzetta, K. M., Chen, H.-W., Fernandez-Soto, A., Pascarelle, S., Yahata, N., & Yahil, A. 1999, in ASP Conf. Ser. 193, The Hy-Redshift Universe, ed. A. J. Bunker & W. J. M. van Breugel (San Francisco: ASP), 544
Lawrence, A., Walker, D., Rowan-Robinson, M., Leech, K. J., & Penston, M. V. 1986, MNRAS, 219, 687
Lilly, S. J., Le Fèvre, O., Hammer, F., & Crampton, D. 1996, ApJ, 460, L1

Lisenfeld, U., Isaak, K. G., & Hills, R. 2000, MNRAS, 312, 433
Madau, P. 1995, ApJ, 441, 18
Madau, P., Ferguson, H. C., Dickinson, M. E., Giavalisco, M., Steidel, C. C., & Fruchter, A. 1996, MNRAS, 283, 1388
Matthews, K., & Soifer, B. T. 1994, in Infrared Astronomy with Arrays, ed. I. McLean (Dordrecht: Kluwer), 239
Meurer, G. R., Heckman, T. M., & Calzetti, D. 1999, ApJ, 521, 64 (MHC)
Oakes, D. 1982, Biometrics, 38, 451
Peacock, J. A., et al. 2000, MNRAS, submitted (astro-ph/9912231)
Pettini, M., Kellogg, M., Steidel, C. C., Dickinson, M., Adelberger, K. L., & Giavalisco, M. 1998, ApJ, 508, 539
Press, W. H., Flannery, B. P., Teukolsky, S. A., & Vetterling, W. T. 1992, Numerical Recipes in C (Cambridge: Cambridge Univ. Press)
Richards, E. A. 2000, ApJ, 533, 611
Rifatto, A., Longo, G., & Capaccioli, M. 1995, A&AS, 114, 527
Rigopoulou, D., Lawrence, A., & Rowan-Robinson, M. 1996, MNRAS, 278, 1049
Rigopoulou, D., Spoon, H. W. W., Genzel, R., Lutz, D., Moorwood, A. F. M., & Tran, Q. D. 1999, AJ, 118, 2625
Sandage, A., & Bedke, J. 1994, The Carnegie Atlas of Galaxies (Washington: Carnegie Inst. Washington)
Sanders, D. B. 1999, Ap&SS, 269, 381
Sanders, D. B., & Mirabel, I. F. 1996, ARA&A, 34, 749
Sanders, D. B., Scoville, N. Z., & Soifer, B. T. 1991, ApJ, 370, 158
Smail, I., Ivison, R. J., & Blain, A. W. 1997, ApJ, 490, L5
Smail, I., Ivison, R. J., Blain, A. W., & Kneib, J.-P. 1998, ApJ, 507, L21
Soifer, B. T., Sanders, D. B., Madore, B. F., Neugebauer, G., Danielson, G. E., Elias, J. H., Lonsdale, C. J., & Rice, W. L. 1987, ApJ, 320, 238
Steidel, C. C., et al. 2000, in preparation
Steidel, C. C., Adelberger, K. L., Giavalisco, M., Dickinson, M., & Pettini, M. 1999, ApJ, 519, 1
Steidel, C. C., & Hamilton, D. 1993, AJ, 10, 2017
Steidel, C. C., Pettini, M., & Hamilton, D. 1995, AJ, 110, 2519
Tan, J. C., Silk, J., & Balland, C. 1999, ApJ, 522, 579
Trentham, N., Blain, A. W., & Goldader, J. 1999, MNRAS, 305, 61
Trentham, N., Kormendy, J., & Sanders, D. B. 1999, AJ, 117, 2152
Xu, C., et al. 1998, ApJ, 508, 576